TÜBİTAK

Turkish Journal of Earth Sciences

http://journals.tubitak.gov.tr/earth/

Review Article

Turkish J Earth Sci
(2022) 31: 520-544
© TÜBİTAK
doi:10.55730/1300-0985.1818

Tectonomagmatic reconstruction of the Upper Mesozoic–Cenozoic Neotethyan arcs in the Lut block, East Iran: a review and synthesis

Reza ARJMANDZADEH[1,*], Saeed ALIREZAEI[2], Alireza ALMASI[3]

[1]Department of Geology, Payame Noor University, Tehran, Iran
[2]Faculty of Earth Sciences, Shahid Beheshti University, Tehran, Iran
[3]Department of Geology, Lorestan University, Khorramabad, Iran

Received: 03.04.2022 • **Accepted/Published Online:** 21.09.2022 • **Final Version:** 16.11.2022

Abstract: The Lut Block in east Iran with a widespread record of arc-type Mesozoic–Cenozoic magmatic rocks is bordered by the Birjand (Sistan) ophiolitic assemblage to the east and the Sabzevar ophiolitic assemblage to the north. The nature and tectonomagmatic setting of these sutures and associated arcs are controversial. The geochemical attributes of the Upper Cretaceous–Paleogene intrusive and extrusive rocks in the central (CLB) and the northern Lut block (NLB) and in the Sabzevar ophiolite zone (SOZ), Late Cretaceous calc-alkaline and adakitic rocks to the east of the Sistan suture (CAS), and the Bazman intrusives to the west are consistent with a subduction-related volcanic arc setting. The Najmabad granitoids in the NLB compositionally overlap with the Eocene Sabzevar calc-alkaline and adakitic lava flows (ESA), implying a common magmatic source and a similar trend of evolution. The island arc basalt-like geochemical patterns and the initial Sr and Nd isotope compositions for the CLB intrusive bodies suggest that the parent magmas formed by partial melting in a suprasubduction mantle wedge. The initial $^{87}Sr/^{86}Sr$ and εNd(t) values for the CAS, the Bazman intrusives, the ESA, and the Najmabad granitoids are similar and overlap those of the Sabzevar ophiolitic rocks. Here, we review the previously proposed one-sided subduction models for the Lut block and the Sabzevar suture zone, and discuss in favour of a two-sided asymmetric subduction as an alternative geodynamic model.

Key words: Lut block, Sistan Ocean, Birjand ophiolite, Sabzevar ophiolite, East Iran, two-sided asymmetric subduction

1. Introduction

The evolution of the Neotethys in Iran was associated with the development of several continental arc and island-arc terrains juxtaposed across several sutures (e.g., Zarrinkoub et al., 2012; Hosseini et al., 2017; Almasi et al., 2019). Most tectonic scenarios concerning the development of the Neotethys portray an active margin along southern Eurasia from mid-Mesozoic through to Cenozoic (e.g., Stampfli and Borel, 2002; Agard et al., 2011; Shafaii Moghadam and Stern, 2015; Stern et al., 2021). In the eastern and northern Lut block in east-northeast Iran (Figure 1), such tectonomagmatic events were associated with the development of extensive arc magmatism and closure of the Neotethyan Sistan and Sabzevar oceanic basins (e.g., Pang et al., 2013; Kazemi et al., 2019).

The Birjand ophiolites to the east of the Lut block (Figure 1) are relicts of the Sistan Ocean that separated the Lut and the Afghan continental blocks during most of the Cretaceous (Babazadeh and De Wever, 2004; Saccani et al., 2010; Zarrinkoub et al., 2012). Several different and contrasting models have been outlined for the closure of the ocean, the emplacement of the ophiolites, and the development of arc-type magmatism, including 1) east-dipping subduction under the Afghan block (Camp and Griffis, 1982; Tirrul et al., 1983); 2) west-dipping subduction under the Lut block (Zarrinkoub et al., 2012); and 3) lithospheric thinning and asthenospheric upwelling associated with the extensional collapse of the east Iranian ranges (Pang et al., 2013).

The east-west trending Sabzevar ophiolitic belt (Figure 1) represents a northern branch of the Neotethys Ocean (Shafaii Moghadam et al., 2015; Rahmani et al., 2020). The belt is bordered to the north by the Alborz zone, also known as Alborz Ranges and Alborz belt, and to the south by the major Dorouneh sinistral strike-slip fault. Extensive outcrops of the Late Cretaceous–Cenozoic calc-alkaline and adakitic rocks occur to the south of the Late Cretaceous Sabzevar ophiolites and extend northwards into the ophiolites (Figure 2).

As for the Sistan basin, there is an ongoing debate as to when and in which direction the Sabzevar oceanic lithosphere subducted. While some authors argue for a

* Correspondence: r.arjmandzadeh@pnu.ac.ir

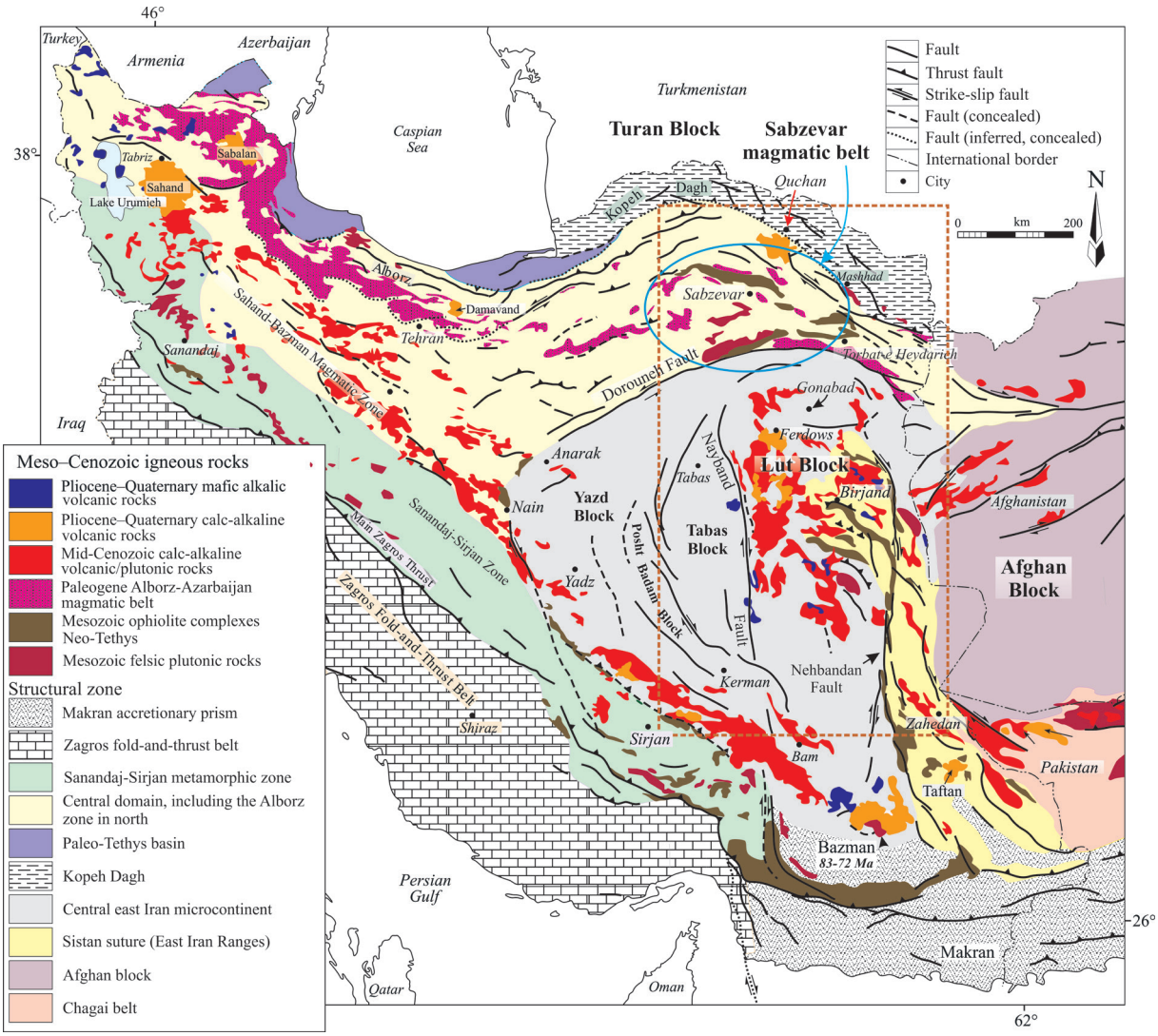

Figure 1. Simplified geological sketch map of Iran, showing the main tectonic blocks/zones and the distribution of Mesozoic and Cenozoic igneous rocks, as well as ophiolitic assemblages (modified from NIOC, 1977; Berberian and King, 1981; Arjmandzadeh et al., 2011; Richards et al., 2012). The dotted square indicates the location of Figure 2, and the blue ellipse highlights the Sabzevar magmatic belt.

Late Cretaceous subduction under the Lut block (e.g., Moix et al., 2008; Shafaii Moghadam and Stern, 2015), others outline an opposite subduction vergence beneath the Turan block at this time (Glennie 2000; Agard et al. 2011).

This paper reviews the contrasting tectonomagmatic scenarios previously proposed for the eastern and northern Lut block using the available geological, geochemical, and geochronological data (Table) on the Upper Mesozoic–Paleogene intrusive and volcanic rocks.

2. Geological background

The Iranian plateau consists of several geological units (Figure 1) delineated by major boundary faults, and/or oceanic suture zones (e.g., Stöcklin, 1976; Berberian and King, 1981). From Late Precambrian to Late Paleozoic times, the proto-crust of Iran was lying to the northeast of the Gondwanaland as an extension of the Afro-Arabian continental platform which then rifted, with the opening of the Neotethys Ocean in Upper Paleozoic, as part of the ribbon continent Cimmeria, (e.g., Stampfli and Borel, 2004; Horton et al., 2008; Alirezaei and Hassanzadeh, 2012).

The Phanerozoic geological evolution of Iran was most influenced by the development of the Neotethys Ocean and subsequent convergence, arc magmatism, and continental collision during Mesozoic–Cenozoic (e.g., Berberian and King, 1982; Bagheri and Stampfli, 2008;

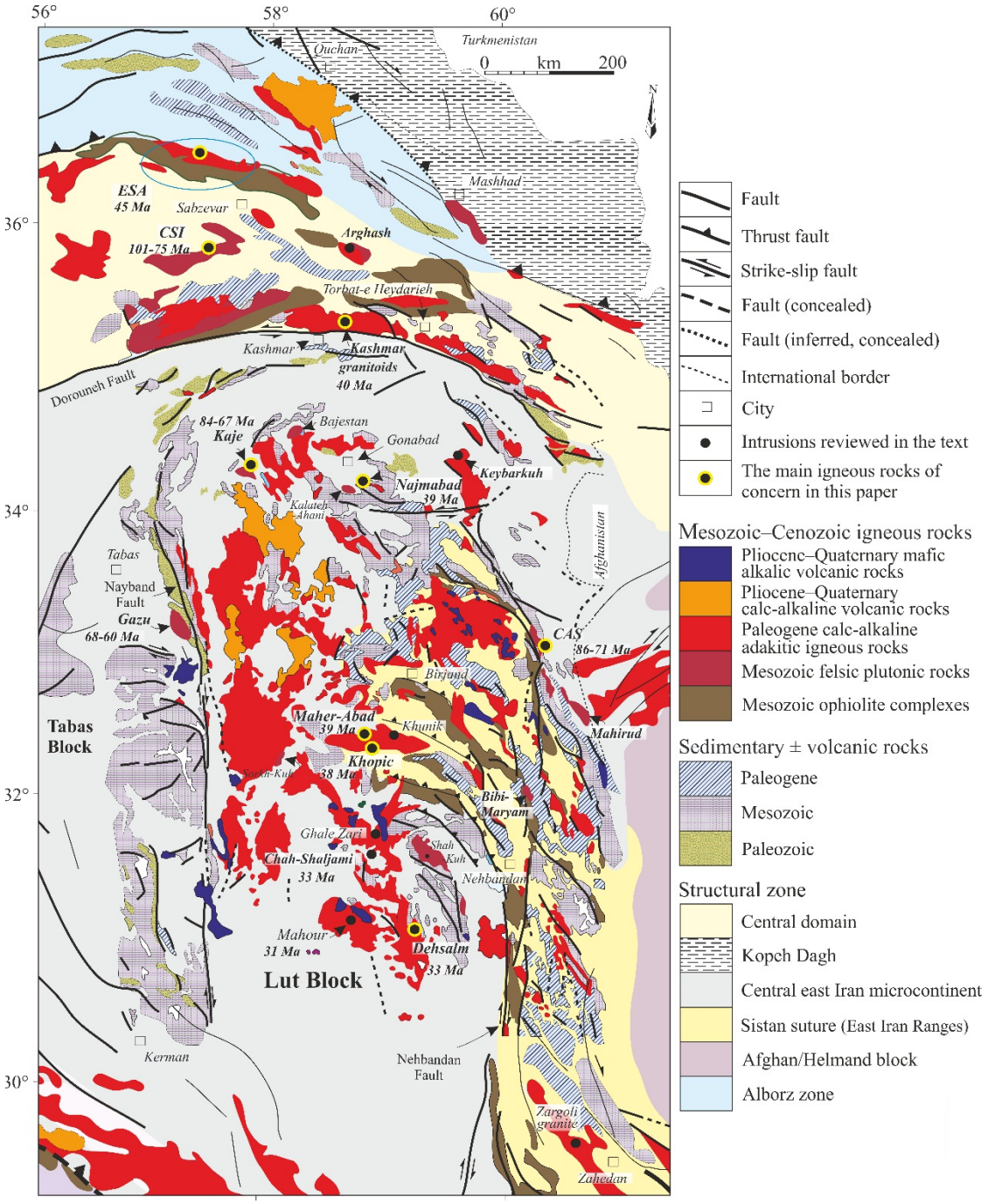

Figure 2. Simplified geological sketch map of the Lut block and the Sabzevar zone, showing the locations of major intrusive bodies (solid circles) discussed in the text (after Berberian and King, 1981; Tirrul et al., 1983; Richards et al., 2012). The blue ellipse indicates the area where the Sabzevar Eocene calc-alkaline and adakites crop out. CSI: The Late Cretaceous Sabzevar intrusive rocks.

Hassanzadeh and Wernicke, 2016). There seems to be a consensus that the Neotethyan subduction in Iran started in the Upper Triassic (e.g., Arvin et al., 2007; Hassanzadeh and Wernicke, 2016). The termination and closure timing of the Ocean was diachronous, and spanned a wide period of time from the Late Cretaceous to as late as the Pliocene (Agard et al., 2011 and references therein).

The triangular terrain in the east central Iran, bordered by ophiolitic assemblages (Figure 1) is known as the central east Iran microcontinent (CEIM) that consists, from west

Table. Summary of the previous geochemical, geochronological, and Sr–Nd isotopic data from CAS, SOZ, NLB, CLB, and the Bazman igneous rocks used for the plots.

Tectonomagmatic zone	Location	Rock type	Radiometric ages	$(^{87}Sr/^{86}Sr)_i$ (n)*	ϵNd_i (n)	Whole rock geochemistry (n)	References
Central Lut block (CLB)	Dehsalm	Gabbro-diorite to granite, with dominance of monzonites and quartz monzonites	33.3 Ma; Rb-Sr whole rock-feldspar-biotite isochron	0.704698–0.705079 (7)	1.52–2.49 (7)	Major oxides and trace element (11)	Arjmandzadeh and Santos, 2014
	Maheraba-Khopic	Monzonitic to dioritic subvolcanic porphyry stocks	39.0 Ma; Zircon U-Pb	0.704756–0.704869 (2)	1.45–1.81 (2)	Major oxides and trace element (6)	Malekzadeh Shafaroudi et al., 2015
Northern Lut block (NLB)	Najmabad	Quartz monzonite and granodiorite	39.9 Ma; Zircon U-Pb	0.705122 (1)	5.16 (1)	Major oxides and trace element (9)	Moradi Noghondar et al., 2012
	Keybarkuh	Monzodiorite, diorite, monzonite, granodiorite, and granite	43.4 Ma; Zircon U-Pb	0.7061–0.7068 (2)	(-3.5)–(-3.6) (2)	No data	Salati et al., 2013
	Kaje	Monzodiorite, monzonite, monzogranite, syenogranite, and granite	84.2, 70.8 and 67.9 Ma; zircon U-Pb	0.706125–0.708080 (3)	(-2.55)–(-7.81) (3)	Major oxides and trace element (10)	Najafi et al., 2014
Southern Lut block	Bazman	Gabbro, diorite, monzodiorite, granodiorite, and porphyritic granites	83.07–72.5 Ma; zircon U-Pb	No data	No data	Major oxides and trace element (15)	Ghodsi et al., 2016
Sabzevar ophiolite zone (SOZ)	Kashmar	Monzogranite, granodiorite, syenogranite, alkali granite, and quartz monzonite	40.2 Ma; Zircon U-Pb	0.705346–0.705761 (3)	(-0.22)–(-1.65) (3)	Major oxides and trace element (12)	Almasi et al., 2019
	Sabzevar calc-alkaline and adakitic lava flows (ESA)	Intermediate to felsic intrusions and volcanic rocks	45–47 Ma; Zircon U-Pb and mica Ar–Ar	0.703563–0.704456 (6)	6.16–6.61 (6)	Major oxides and trace element (15)	Shafaii Moghadam et al., 2016
	Late Cretaceous Sabzevar intrusive rocks (CSI)	Diorite, gabbrodiorite and granite	101.9–75.7 Ma; Zircon U-Pb	0.70423–70579 (14)	5.81–7.22 (14)	Major oxides and trace element (11)	Kazemi et al., 2019
Eastern side of the Sistan suture	Late Cretaceous calc-alkaline and adakitic rocks to the east of the Sistan suture (CAS)	Low-K calc-alkaline rocks and intermediate to felsic high-silica adakitic rocks	86.0–71.5 Ma; K-Ar dating of tonalitic rocks (Maurizot et al., 1990) and zircon U-Pb (Zarrinkoub et al., 2010)	0.704018–0.707407 (11)	2.0–6.7 (11)	Major oxides and trace element (15)	Jentzer et al., 2020

* (n): Number of representative analyses used for the plots.

to east, of Yazd, Posht Badam, Tabas, and Lut blocks separated by major boundary faults. There is stratigraphic and paleomagnetic evidence that from the Upper Triassic through to Quaternary, the CEIM experienced an approximately 135° counterclockwise rotation with respect to Eurasia (Davoudzadeh and Weber-Diefenbach, 1987; Soffel et al., 1996), with the Late Triassic-Middle Jurassic accounting for approximately 65° of the rotation (Soffel et al., 1996).

During the Middle to Upper Jurassic transition (approximately 165 to approximately 161 Ma), several large granitoid complexes, including the Kalateh-Ahani, Shah-Kuh and Sorkh-Kuh (Moradi Noghondar et al., 2011; Esmaeily et al., 2005; Karimpour et al., 2011) were intruded into the Upper Triassic-Lower Jurassic shales and sandstones of the Shemshak Formation, or Shemshak group (Figure 3).

During Upper Jurassic-Cretaceous, the CEIM experienced a further counterclockwise rotation of 35° (Soffel et al., 1996). The Cretaceous was a time of syn-collisional magmatism in the Lut block that is marked by the intrusion of Bajestan and Kaje granitoids, as well as a second intrusive body in the Kalateh-Ahani (see Section 2.2 for explanation).

The CEIM experienced an additional rotation of 35° during the Cenozoic, summing up to approximately 135° counterclockwise rotation with respect to Eurasia since the Upper Triassic (Mattei et al., 2012). The Cenozoic magmatic assemblages in the Lut block thus underwent a maximum counterclockwise rotation of 35°, with the younger suites experiencing a lower rate of rotation. The youngest magmatic manifestation in the Lut block involved the emplacement of the Neogene–Quaternary alkali olivine basalts along major boundary faults (Figure 2).

The Lut block is bordered by the Sabzevar magmatic belt and the Kopeh-Dagh Ranges to the northeast, and by the Alborz zone to the north that is itself bordered by the Turan block northward (Figures 1 and 2). The Lut block is bounded to the east by the Sistan suture and Nehbandan, or simply Neh, fault, to the west by the Nayband fault, and to the south by the Makran accretionary prism

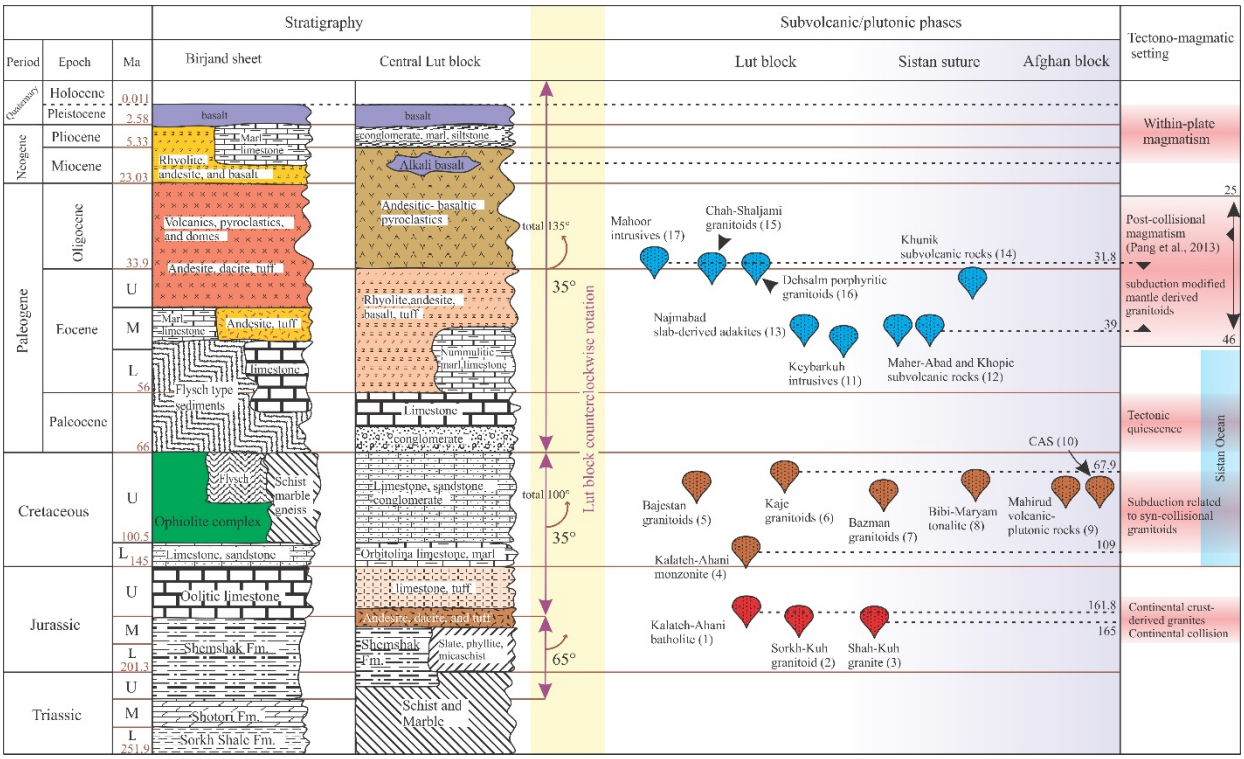

Figure 3. Synoptic chronostratigraphic-tectonic scheme summarizing the geological evolution of the Lut block. The stratigraphic columns are summarized from the Dehsalm and Birjand 1:250,000 geological maps (Geological Survey of Iran, 1992a, 1992b). The counterclockwise rotation rate of the Lut block is indicated after Soffel et al. (1996). The tectonic setting and chronology data on granitoids are from: 1 and 2: Karimpour et al., 2011; 3: Esmaeily et al., 2005; 4: Karimpour et al., 2014; 5: Ahmadi-Rouhani et al., 2017; 6: Najafi et al., 2014; 7: Ghodsi et al., 2016; 8: Zarrinkoub et al., 2010; 9: Keshtgar et al., 2019; 10: Jentzer et al., 2020; 11: Salati et al., 2013; 12: Malekzadeh Shafaroudi et al., 2015; 13: Moradi Noghondar et al., 2012; 14: Samiee et al., 2016; 15: Arjmandzadeh et al., 2011; 16: Arjmandzadeh and Santos, 2014; and 17: Beydokhti et al., 2015.

(Figure 2). The block features a pre-Jurassic metamorphic basement, Jurassic shales, sandstones, and carbonates, Late Cretaceous ophiolites, and extensive outcrops of late Mesozoic and Cenozoic intrusive and volcanic rocks (Camp and Griffis, 1982; Tirrul et al., 1983).

The Sabzevar ophiolite zone (SOZ) to the north of the Lut block extends for over 400 km in an east–west direction and is bounded to the north by the Alborz zone and to the south by the Dorouneh fault (Figure 2). The SOZ is known to represent an orogenic suture zone created in the course of the closure of the Cretaceous Sabzevar Ocean that developed in the back-arc domain of the Neotethyan subduction (Bagheri and Stampfli, 2008; Rossetti et al., 2010). Shafaii Moghadam and Stern (2015) presented geochemical, geochronological, and paleontological evidence that the Sabzevar Ocean existed from at least mid-Cretaceous times between the Turan block to the north and the Lut Block to the south.

The Mesozoic–Cenozoic stratigraphy and tectonomagmatic episodes in the Lut Block are summarized in a synoptic chronostratigraphic-tectonic scheme (Figure 3). The central and eastern Lut block experienced different history of tectono-magmatism and thus record different geological fingerprints. The Birjand sheet best represents the Sistan suture zone that embraces ophiolitic assemblages, an accretionary prism, and high-pressure/low-temperature metamorphic rocks, while the Dehsalm sheet best defines the central Lut block with a profuse record of Mesozoic–Cenozoic magmatism. Two stratigraphic columns are thus presented in Figure 3, one for the Birjand sheet and the other for the Central Lut block. A description of various magmatic rocks in the Lut block and in the Sabzevar ophiolite zone and the East Sistan suture and the Afghan block is presented in the following sections.

2.1. Central Lut block

Magmatism in the Central Lut is dominated by lower-middle Eocene andesitic and basaltic lava flows and pyroclastic rocks, and middle-to-late Eocene–Oligocene porphyritic subvolcanic intrusions represented by Maherabad-Khopic, Chah-shaljami, Dehsalm and Mahour (Malekzadeh Shafaroudi et al., 2015; Arjmandzadeh et al., 2011; Arjmandzadeh and Santos, 2014; Beydokhti et al., 2015).

The volcanic rocks in the Chah-shaljami area are intruded by a set of granodiorite and quartz monzodiorite dykes, as well as quartz monzonite and granodiorite stocks (Figure 2). A Rb–Sr age of 33.5 ± 1 Ma, mainly dependent on the Sr isotopic composition of biotite, was obtained in a quartz monzonite sample, consistent with early Oligocene (Arjmandzadeh et al., 2011).

The Dehsalm intrusive complex consists of multiple intermediate to felsic and subordinate mafic intrusions (Figure 2). A consistent whole rock, feldspar, and biotite Rb–Sr age of 33 ± 1 Ma was obtained from a quartz monzonite sample that coincides, within error, with that of Chah-Shaljami granitoids (Arjmandzadeh and Santos, 2014).

The Mahour intrusions (Figure 2) occurring as stocks and dykes consist mainly of gabbrodiorite, diorite, monzodiorite, and tonalite. A diorite sample yielded zircon U-Pb age of 31.88 ± 0.2 Ma (Beydokhti et al., 2015).

2.2. Northern Lut block

The uppermost Lower and Upper Cretaceous granitoids in the northern Lut block are represented by the Kalateh-Ahani (109 ± 1 and 108.7 ± 0.6 Ma), Kaje (84.2 ± 1.3, 70.8 ± 1.4 and 67.9 ± 1Ma) and Bajestan (79.03 ± 1.1–76.04 ± 0.37 Ma), all dated by zircon U-Pb method, which were intruded into the Upper Triassic-Lower Jurassic metamorphosed shales and sandstones of the Shemshak Formation and the Cretaceous limestones and marls (Karimpour et al., 2014; Najafi et al., 2014; Ahmadi-Rouhani et al., 2017).

Karimpour et al., (2014) reported $(^{87}Sr/^{86}Sr)_i$ and ϵNd_i isotopic ratios ranging from 0.710897 to 0.717908 and from –7.38 to –10.65, respectively, for the intrusive bodies in Kalateh-Ahani, implying a significant contribution of crustal materials in the development of the parent magma.

The whole rock geochemical attributes and the $(^{87}Sr/^{86}Sr)_i$ and ϵNd_i isotopic ratios for the Bajestan intrusives (0.710897–0.717908 and –7.38 to –10.65, respectively) suggest a crustal source for the parental magma (Ahmadi-Rouhani et al., 2017).

Mahdavi et al. (2016) reported zircon U-Pb ages of 68.1 ± 1.7 to 60.2 ± 1.2 Ma for the Gazu intrusive bodies in the Tabas block near the boundary with the Lut block (Figure 2). The intrusions, hosted in the Triassic dolomite and Jurassic shales and sandstones, are described as high-K calc-alkaline and metaluminous to weakly peraluminous granitoids formed in a volcanic arc setting (Mahdavi et al., 2016).

The Najmabad Eocene intrusive complex (Figure 2) in the northern Lut block consists of several shallow porphyritic intrusions described as hornblende-monzonite, hornblende-biotite monzonite and biotite-monzonite intruded into the Jurassic schist and hornfels, and into the Middle Jurassic Najmabad/Kalateh-Ahani granitic batholith (Moradi Noghondar et al., 2012; Karimpour et al., 2011). A chemical classification of the rocks indicates that they are mainly granodiorite and quartz monzonite (see Section 3.1 for discussion). Zircon U–Pb dating of a monzonitic stock yielded a crystallization age of approximately 39.9 ± 1.5 Ma, corresponding to middle Eocene (Moradi Noghondar et al., 2012).

The Keybarkuh intrusive complex in the northern Lut block (Figure 2) includes several Cretaceous–Cenozoic

subvolcanic intrusions occurring as stocks and dykes intruded into Paleozoic slates, phyllites, and schists (Salati et al., 2013). A granodiorite porphyritic intrusion yielded a zircon U-Pb age of 43.4 ± 0.33 Ma corresponding to middle Eocene (Salati et al., 2013).

2.3. Bazman intrusive complex (southern Lut block)

The Bazman intrusive complex in the southernmost Lut block (Figure 1) and west of the Sistan suture zone consists of a large zoned pluton intruded into the upper Paleozoic shales, sandstones, and limestones. The intrusive rocks range in composition from felsic to intermediate and mafic, and belong to the I-type magmatic series (Ghodsi et al., 2016). Zircon U-Pb dating on the more felsic fractions (granite, granodiorite, and monzodiorite) indicated a time span of 83.07 ± 0.30–72.50 ± 0.1 Ma, consistent with Late Cretaceous, for the emplacement of the intrusions (Ghodsi et al., 2016).

2.4. Eastern Sistan suture and Afghan block

Jentzer et al. (2020) reported the occurrence of two coexisting sets of arc type volcanic–plutonic assemblages consisting of low-K calc-alkaline basaltic to rhyolitic lava flows and intermediate to felsic high-silica adakitic intrusions in the Afghan block to the east of the Sistan suture (Figure 2). K-Ar dating of tonalitic rocks (Maurizot et al., 1990) and zircon U-Pb dating of adakitic granitoids (Zarrinkoub et al., 2010) suggest an emplacement age of 86 ± 0.8 to 71.5 ± 0.6 Ma for the magmatic suite. Jentzer et al. (2020) linked the development of the arc to NE-dipping subduction of the Sistan oceanic lithosphere under the Afghan margin in the Upper Cretaceous (Figure 2).

2.5. Sabzevar ophiolite zone

Extensive outcrops of a Cretaceous–Cenozoic magmatic suite consisting of mafic to felsic volcanic, volcanoclastic, subvolcanic, and plutonic rocks occur in the Sabzevar ophiolite zone (SOZ), also known as Sabzevar structural zone and Sabzevar suture zone (Figure 2). The SOZ also hosts several plagiogranite bodies occurring as lenses, veins, dykes, and small pods enclosed in layered gabbro, harzburgites, and sheeted dykes (Shafaii Moghadam et al., 2015).

The SOZ magmatic suite occurs mostly to the south of the Late Cretaceous Sabzevar ophiolites, but scattered exposures of similar rocks occur also within the ophiolites and to the north (Figure 2). Dacitic to rhyolitic lava flows and subvolcanic domes cover large areas in the SOZ (Shafaii Moghadam et al., 2015).

A thick sequence of volcano-sedimentary rocks in southwest Sabzevar is intruded by Late Cretaceous Sabzevar intrusive rocks (CSI) consisting of hypabyssal granitoid and gabbroic bodies. Zircon U-Pb dating of the intrusive and volcanic rocks yielded ages ranging between 101.9 ± 1 and 75.78 ± 0.29 Ma (Kazemi et al., 2019). The authors linked the Late Cretaceous, nonophiolitic Sabzevar magmatic rocks to partial melting of a MORB-type slab or depleted-mantle wedge during the north-verging subduction of the Sabzevar oceanic slab under the Turan block.

The southern Quchan magmatic arc to the north of the Sabzevar ophiolitic assemblage (Figure 2) embraces widespread Cenozoic intermediate-felsic calc-alkaline and adakitic domes, intrusive bodies, and volcanic rocks with the ages younging northward from Sabzevar ophiolitic assemblage towards Quchan (Shabanian et al., 2012). While the Eocene adakitic suite of this arc (Figures 1 and 2) formed in a continental margin setting, the Oligocene–Miocene and Plio-Pleistocene adakitic domes and dykes are linked to lithospheric delamination, possibly due to a slab break-off (Omrani et al., 2018). Gardideh et al. (2018) reported zircon U–Pb ages of 17.83 ± 0.24 Ma and 8.50 ± 0.34 Ma for the emplacement of the adakitic rocks in the south Quchan.

The Kashmar subvolcanic and plutonic bodies (KSP) occur in the southernmost part of the Sabzevar magmatic belt at close proximity to the Dorouneh fault (Figure 2). The geology of the Kashmar area is marked by Paleocene–Eocene silicic to mafic lava flows and middle Eocene granitoid bodies (Almasi et al., 2019). The granitoids consist mainly of monzogranite, granodiorite, syenogranite, alkali granite, and minor quartz monzonite (Almasi et al., 2019). The quartz monzonite yielded a zircon U–Pb age of 40.2 ± 0.3 Ma corresponding to middle Eocene (Almasi et al., 2019).

3. Geochemistry of the CAS, SOZ, NLB, CLB, and the Bazman igneous rocks

Magmatism in the Lut block and the Sabzevar ophiolite zone is most represented by the felsic-intermediate and subordinate mafic intrusive and volcanic rocks of the Late Cretaceous–Paleogene times, a critical period in the evolution of the block and the main focus of the present study. Limited outcrops of Miocene and Plio-Pleistocene magmatic rocks do occur in the Lut block and Sabzevar zone that are briefly discussed using the available data.

3.1. Major element geochemistry

3.1.1. Late Cretaceous igneous rocks

On the total alkali-silica diagram (Le Maitre, 2002), the CAS and the Bazman intrusives display a wider range of composition, from mafic to felsic, compared to those of the CSI intrusives and the Kaje granitoid complex in the NLB (Figure 4A). The CSI rocks are dominated by gabbrodiorite and granite. The Kaje complex consists mainly of intermediate to felsic rocks ranging in compositions from diorite to monzonite, quartz monzonite, and granite.

The Kaje and Bazman intrusive bodies display higher K_2O contents (mean 4.13 and 2.39 wt.%, respectively)

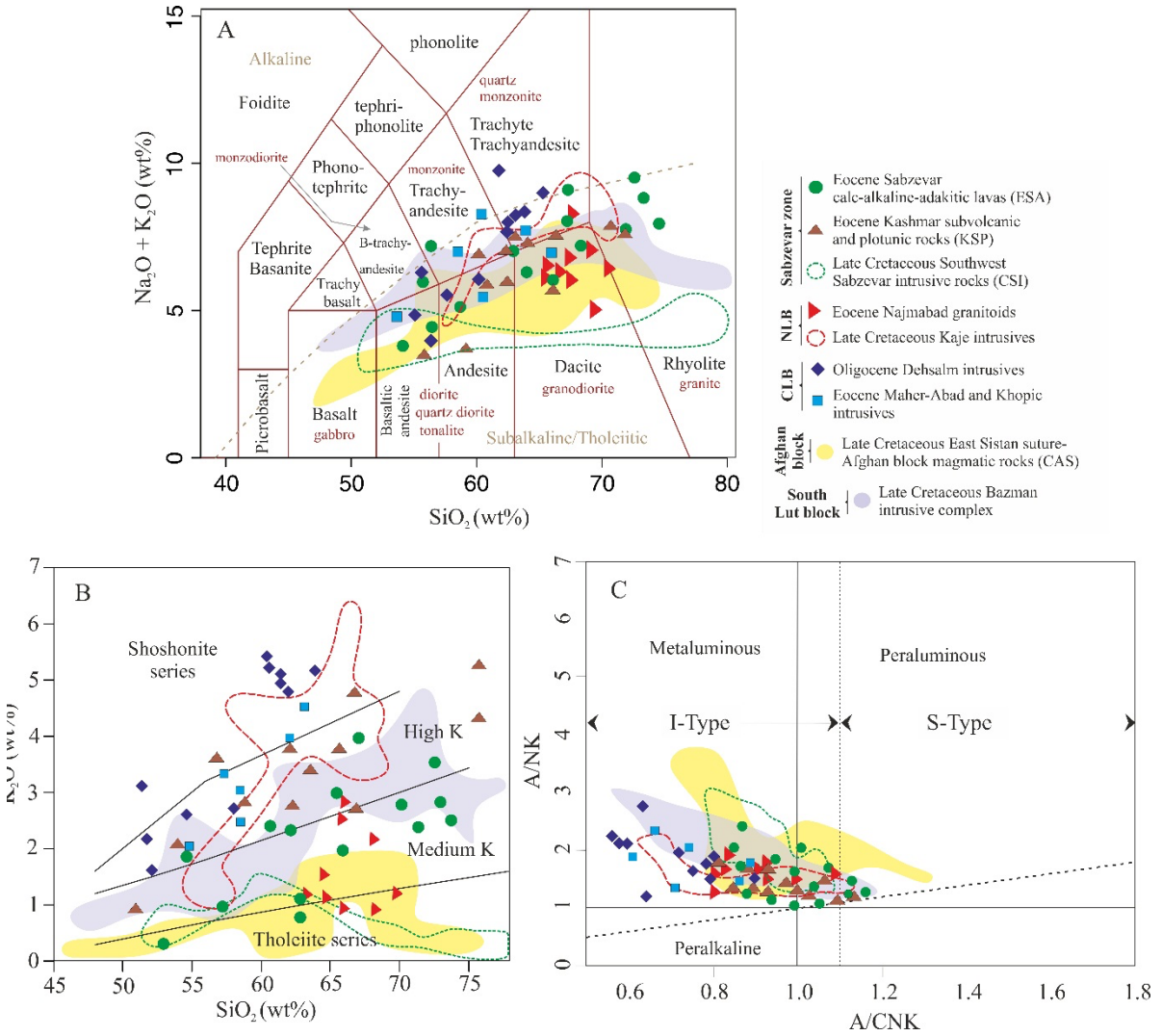

Figure 4. Plots of the CAS, SOZ, NLB, CLB, and the Bazman igneous rocks on: (A) Total alkali-silica diagram of Le Maitre (2002). The intrusive equivalents of volcanic rocks are also indicated. The dotted line for the alkaline/subalkaline series divides after Irvine and Baragar (1971). (B) A/NK [molar $Al_2O_3/Na_2O + K_2O$] vs. A/CNK $Al_2O_3/(CaO + K_2O + Na_2O)$] diagram of Maniar and Piccoli (1989). The boundaries between I- and S-type and metaluminous and peraluminous granitoids after Chappell and White (1992) and Chappell and White (1974), respectively. (C) K_2O vs. SiO_2 diagram of Peccerillo and Taylor (1976). Refer to Table for the sources and number of representative analyses used for the plots.

compared to those of the CAS and CSI intrusions (mean 0.65 and 1.04 wt.%, respectively) (Figure 4B). On the A/NK vs. A/CNK diagram, all intrusive rocks plot in the metaluminous field, with few samples from CAS and CSI extending into the peraluminous domain (Figure 4C). The magnesium number [Mg# = 100*Mg/(Mg + Fe), using atomic ratios] ranges between 38.9 and 67.7 for the CAS, 22.3 and 48 for the CSI, 26.3 and 53.2 for the Bazman, and 16.7 and 54 for the Kaje igneous rocks

3.1.2. Paleogene igneous rocks

The CLB intrusive bodies plot in the gabbro-diorite, diorite, monzonite, monzodiorite, quartz monzonite, and granodiorite fields (Figure 4A). The felsic high-silica Najmabad intrusions plot mainly in the granodiorite and quartz monzonite fields. The intrusions were described by Moradi Noghondar et al. (2012) as monzonite based on petrographic specifications. The Eocene Sabzevar calc-alkaline and adakitic lava flows (ESA) are subalkaline and span a range of composition from basaltic-andesite to rhyolite (Figure 4A). The ESA and the Kashmar intrusive bodies within the SOZ display a broader compositional range with respect to those of the CLB and NLB intrusions.

The Paleogene magmatic suites from CLB, NLB, and SOZ are metaluminous; the SOZ rocks extend partly into

the peraluminous domain (Figure 4C). The Najmabad granitoids correspond to the field defined by the Eocene Sabzevar adakitic lava flows (ESA). On the K_2O vs. SiO_2 discrimination diagram (Peccerillo and Taylor, 1976), the Najmabad granitoids and the Sabzevar zone rocks fall mainly in the medium-to-high K calc-alkaline domain, whereas the CLB and KSP intrusions plot in the high-K calc-alkaline to shoshonitic domains (Figure 4B). The CLB intrusives are distinguished by higher K_2O contents (1.64–5.65 wt.%) compared to those of the NLB (0.9–2.82 wt.%) and SOZ (0.27–3.81 wt.%) magmatic rocks. The magnesium numbers are relatively high for the Dehsalm (40.1 to 55.6) and the Kashmar intrusives (42.6 to 61.6) compared to Maherabad-Khopic (31.9–43.4) and Najmabad intrusives (12.8–50.5) and the ESA volcanic rocks (11.5–61.4).

3.2. Minor and trace element geochemistry

3.2.1. Late Cretaceous igneous rocks

The Late Cretaceous intrusive rocks from the Sabzevar zone and the Lut and Afghan blocks display large variations in composition and can be classified into mafic, intermediate, and felsic groups (Figure 5A–5F). Such treatment of the geochemical data helps better investigate the source and evolution of the parent magmas. The least differentiated rocks, represented by the mafic group, best represent the source areas (mantle vs. crustal sources). The more evolved intermediate and felsic groups display patterns that are generally influenced by differentiation and/or contribution from crustal materials or crustal contamination.

The least evolved rocks of the CSI and the Bazman intrusive complex exhibit depletions in high field strength elements, Nb, Zr, and Ti, but enrichments in large ion lithophile elements, Th, U, K, and Sr (Figure 5D). These features can be explained by partial melting of a mantle metasomatized by subduction fluids (i.e. Peccerillo and Lustrino, 2005; Seghedi and Downes, 2011).

None of the mafic rocks representing the Late Cretaceous CAS, CSI, NLB, and Bazman igneous rocks display negative Eu anomalies (Figure 5A). This is also the case for the CAS and CSI intermediate and the CAS and Bazman most evolved rocks (Figures 5A–5C).

On the Rb vs. (Nb+Y) tectonomagmatic discrimination diagram (Pearce et al., 1984), the CAS and CSI rocks and the Bazman intrusives fall in the volcanic arc granite field (Figure 6A). The Kaje intrusions plot in the VAG and syn-collision domains. These intrusions plot in the VAG domain on the Zr-Nb-Ce/P_2O_5 discrimination diagram of Muller and Groves (1997) (Figure 6B). In Sr/Y vs. Y and $(La/Yb)_N$ vs. $(Yb)_N$ discrimination diagrams (Figure 6C and 6D), the intrusive bodies plot in both adakitic and normal arc andesite-dacite-rhyolite domains.

3.2.2. Paleogene igneous rocks

Chondrite-normalized REE and primitive mantle-normalized multielement plots for the CLB intrusive rocks are compared to those for the NLB and the Eocene Sabzevar calc-alkaline and adakitic rocks in Figures 7A–7F. The patterns are broadly similar, with enrichments in large ion lithophile elements (LILE) relative to high field strength elements (HFSE) and negative Nb and Ti anomalies. Distinct differences, however, exist among the various sample groups that can be explained by the source and evolution paths of the parent magmas. The KSP rocks display less steep patterns compared to those of the Najmabad granitoids and the ESA rocks (Figures 7D–7F).

The lower Nb, Ta, and Ti, and higher Sr contents in the CLB and ESA mafic rocks can be explained by the absence of plagioclase and presence of Fe–Ti oxides in the source area (c.f. Martin, 1999). The Nb and Ta depletion in arc magmas can be attributed to earlier depletion of the metals in the source area (e.g., Gust et al., 1997). The negative anomalies for Ti and P in the CLB, NLB, and ESA felsic rocks can be explained by fractionation of Fe-Ti oxides and apatite, respectively (e.g., Mason and McDonald 1978).

The CLB intrusive rocks display broadly similar patterns with strong enrichments in LILE and flat HREE profiles (Figures 7A–7C). The geochemical fingerprints of the parental magmas can be explained by phlogopite breakdown and the presence of refractory garnet in the mantle source (c.f. Ionov and Hofmann, 1995). The Najmabad granitoids and the ESA rocks display features typical of subduction-related magmas, similar to those described for calc-alkaline volcanic rocks from active continental margins (e.g., Walker et al., 2001; Castillo, 2012).

All KSP samples, from the least to most evolved fractions, display negative Eu anomalies (Figures 7A–7C). Lack of distinct Eu anomalies, as in the ESA rocks and the Najmabad intrusions, either suggests that plagioclase fractionation was not significant, or a combination of hornblende and plagioclase fractionation occurred in a ratio appropriate to prevent significant Eu anomaly (e.g., Martin, 1999; Eyuboglu et al., 2011).

Negative Eu anomalies, as displayed by the KSP rocks, can be explained by fractional crystallization of the early, Ca-rich plagioclases (e.g., Rollinson, 1993; Eyuboglu et al., 2011), and/or the oxidized nature of the magma, as discussed earlier in Section 2.3. Under oxidizing conditions, Eu occurs dominantly as Eu^{3+}, leaving lesser Eu^{2+} to be incorporated into plagioclase (Cherniak and Dimanov, 2010). This would explain the lack of evident negative Eu anomalies in the CLB intrusive rocks.

On the Rb vs. (Nb+Y) tectono–magmatic discrimination diagram (Pearce et al., 1984), all samples fall in the volcanic arc granite field (Figure 6A). The Dehsalm and Kashmar intrusions plot in the VAG domain with a tendency toward syn-collision and within-plate domains (Figure 6A). The same intrusions plot in the postorogenic domain on the Zr-

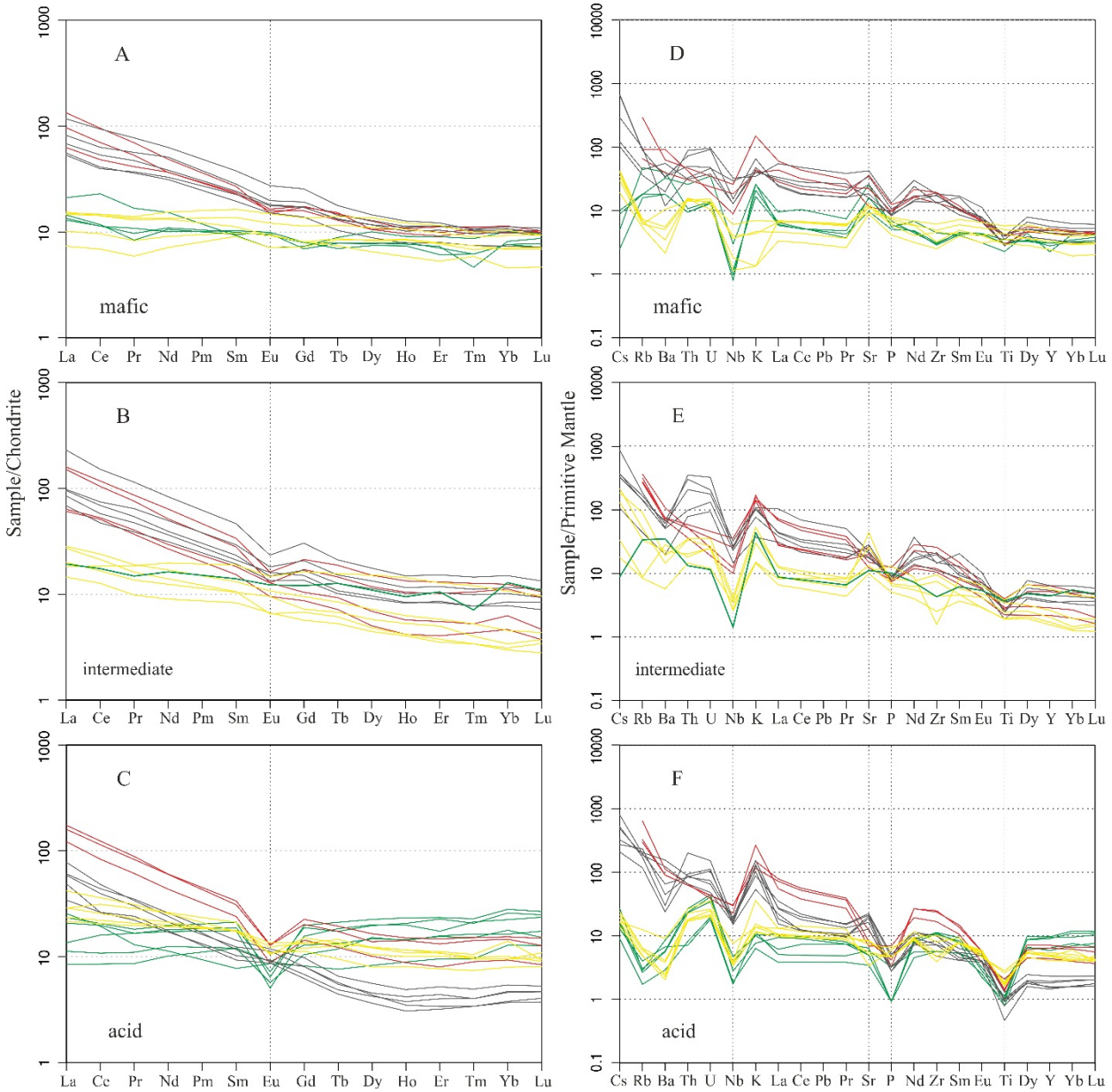

Figure 5. (A–C) Chondrite–normalized rare earth elements, and (D–F) primitive mantle-normalized multielement diagrams for the Late Cretaceous CAS, CSI, Kaje, and the Bazman igneous rocks. The chondrite and primitive mantle values after Boynton (1984) and Sun and McDonough (1989), respectively. Symbols are as in Figure 4. Refer to Table for the sources of data.

Nb-Ce/P_2O_5 discrimination diagram of Muller and Groves (1997) (Figure 6B). Such overlaps or discrepancy of plots in discrimination diagrams is not uncommon, and this requires the interpretations to be validated by other lines of evidence. This is discussed in the following sections. The Najmabad granitoids overlap the Sabzevar suite and plot away from other samples in both diagrams.

In Sr/Y vs. Y discrimination diagram (Figure 6C), the CLB intrusive bodies plot in both adakite-like and normal arc andesite-dacite-rhyolite domains. In the $(La/Yb)_N$ vs. $(Yb)_N$ diagram (Figure 6D), the rocks plot within or towards the normal arc field. Despite some similarities with adakitic rocks, including high Sr/Y ratios, the CLB intrusions are distinct from normal adakites by higher K_2O and K_2O/Na_2O ratios, and lower $(La/Yb)_N$ and $(Ce/Yb)_N$. The high Sr/Y ratios result from the elevated Sr content which is common also in modern high-K to shoshonitic arc magmas (e.g., Moyen, 2009).

In contrast to the CLB and the Kashmar intrusives, the ESA lava flows and Najmabad intrusions plot consistently

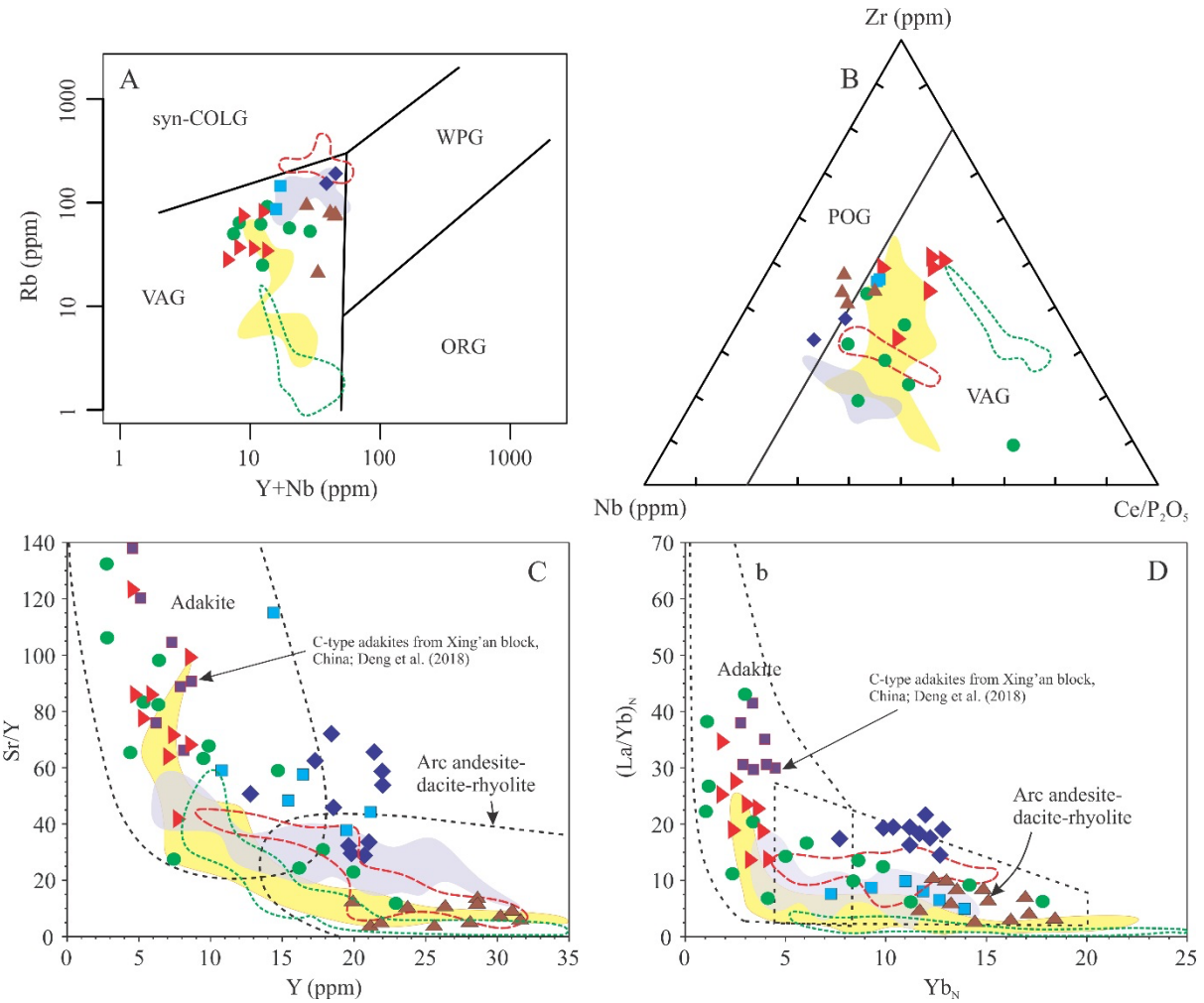

Figure 6. (A,B) Plots of the CAS, SOZ, NLB, CLB, and the Bazman igneous rocks on the geotectonic setting discrimination diagrams of Pearce et al. (1984) and Muller and Groves (1997), respectively, for granitoid rocks. WPG: within plate granites, VAG: volcanic arc granites, ORG: ocean ridge granites, syn-COLG: syncollisional granites, POG: postorogenic granites. (C,D) Plots of the same rocks on the Sr/Y vs. Y and $(La/Yb)_N$ vs. $(Yb)_N$ diagrams for discriminating adakitic rocks from normal arc dacites and rhyolites. Fields for adakite and normal arc dacites and rhyolites adopted from Castillo (2006, 2012) and Defant and Drummond (1990). Symbols are as in Figure 4. Refer to Table for the sources of data.

within the fields of adakite like rocks. The Kashmar samples fall mainly in the field of normal arc andesite-dacite-rhyolite in both Sr/Y vs. Y and $(La/Yb)_N$ vs. $(Yb)_N$ diagrams.

4. Sr–Nd isotope systematics

The initial $^{87}Sr/^{86}Sr$ and ϵNd_i values for Maherabad-Khopic, Dehsalm, and Chah-shaljami intrusive complexes vary from 0.70470 to 0.70506 and +1.4 to +2.7, respectively. On the εNd vs. $(^{87}Sr/^{86}Sr)_i$ diagram (Figure 8), the intrusions plot to the right of the so-called mantle array and straddle the boundary of island-arc basalts (IAB). The IAB-like isotopic compositions of the four intrusive complexes suggest that the parental magmas formed by partial melting in a suprasubduction mantle wedge (c.f., DePaolo and Wasserburg 1976; Conticelli et al., 2009). A mantle source is further supported by the occurrence of gabbroic rocks in the Dehsalm area.

A common source and evolution path for the Dehsalm and Chah-shaljami intrusives are inferred from the very similar initial Sr and Nd isotopic compositions and the geochemical fingerprints. Malekzadeh Shafaroudi et al. (2015) consider the isotopic values for the Maherabad-Khopic intrusives as indicative of oceanic slab-derived magmas.

The initial $^{87}Sr/^{86}Sr$ ratios for the Kashmar and Keybarkuh granitoids, ranging from 0.7053 to 0.7061 and 0.7061 to 0.7068, as well as the negative εNd values

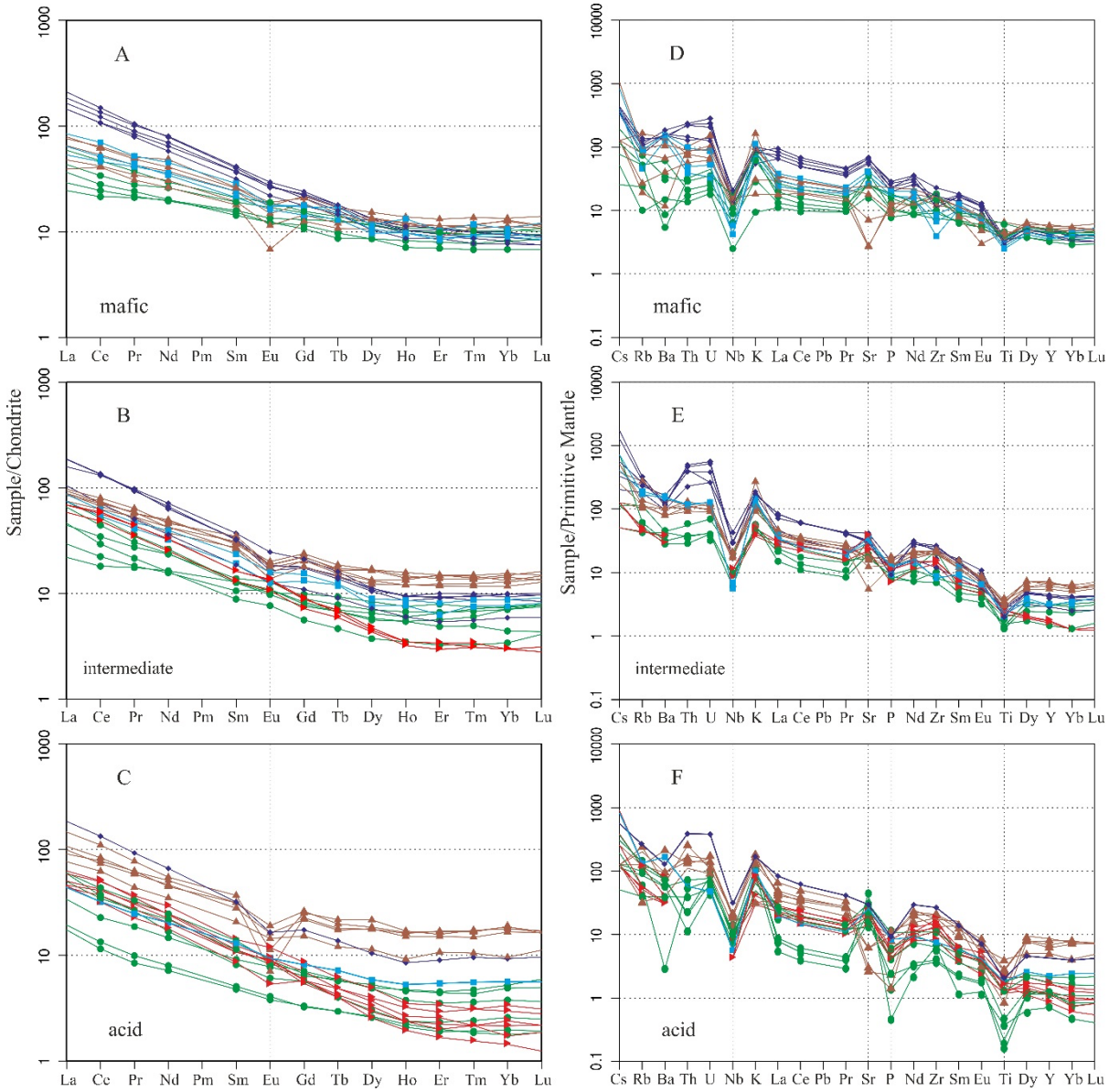

Figure 7. (A–C) Chondrite-normalized rare earth elements, and (D-F) primitive mantle-normalized multi-element diagrams for the CLB, NLB, and SOZ Paleogene rocks. The chondrite- and primitive mantle- normalization values after Boynton (1984) and Sun and McDonough (1989), respectively. Symbols are as in Figure 4. Refer to Table for the sources of data.

varying from −1.65 to −0.02 and −3.5 to −3.6, respectively (Figure 8), are consistent with a depleted MORB mantle (N-MORB) source contaminated by crustal materials (e.g., Müntener et al., 2004).

The initial $^{87}Sr/^{86}Sr$ and εNd(t) values for the Najmabad granitoids in the northern Lut block are 0.70512 and +5.1, respectively, consistent with those of the ESA rocks. All samples plot within the range representing the Sabzevar ophiolitic rocks, implying a common source. The relatively high εNd(t) ratios for the Najmabad samples suggest that parental magmas originated from a subduction-modified depleted mantle (e.g., Stern and Kilian, 1996), similar to the same mantle source for the Sabzevar ophiolites.

The calculated Nd model ages (TDM; DePaolo, 1981) for the Sabzevar volcanic rocks and the Najmabad granitoids range between 0.21 and 0.36 Ga, implying the involvement of a relatively young continental lithosphere in the formation of the Sabzevar and Najmabad suites of rocks (Moradi Noghondar et al., 2012; Shafaii Moghadam et al., 2016). The model ages are distinguished from the Nd model ages for the Kashmar and Keybarkuh granitoids with TDMs at 0.71–0.85 and 0.84 Ga., respectively, which

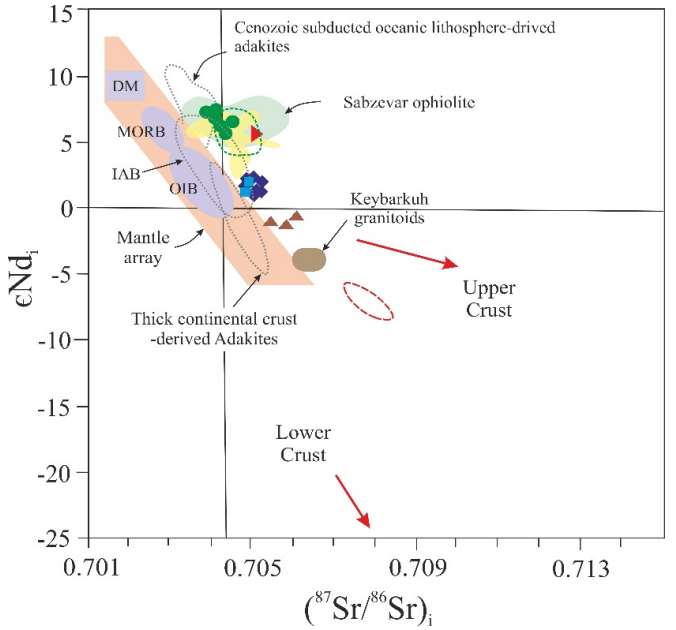

Figure 8. The ϵNd_i-($^{87}Sr/^{86}Sr)_i$ diagram for the CLB, NLB, and KSP intrusive bodies and the Sabzevar volcanic rocks. The field for Cenozoic subducted oceanic lithosphere-derived adakites is defined after Defant et al. (1992), Kay et al. (1993), Sajona et al. (2000), and Aguillón-Robles et al. (2001). The field for adakitic rocks derived from the thickened continental crust is adopted from Muir et al. (1995) and Petford and Atherton (1996). The field for the Sabzevar ophiolites and the ESA lavas are from Shafaii Moghadam et al., 2015 and 2016, respectively. Refer to Table for the sources and number of representative analyses used for the plots. Fields for MORB (Mid-ocean ridge basalts), DM (Depleted mantle), OIB (Ocean-island basalts), and IAB (island arc basalts) after Zindler and Hart (1986). The mantle array is from DePaolo and Wasserburg (1979). Symbols are as in Figure 4.

suggest the involvement of older sources (Almasi et al., 2019; Salati et al., 2013). The isotope geochemistry and the TDM data for the Sabzevar Paleogene granitoids and those for the northern Lut block magmatic belt indicate similarities between the two suites of rocks.

5. A review of the tectonomagmatic models

Several geodynamic models involving different subduction polarity have been proposed for the Upper Cretaceous–Cenozoic evolution of the Lut block and the Sabzevar zone. A review of the models is presented in the following sections.

5.1. Lut block

5.1.1. E- ENE-dipping subduction beneath the Afghan block

Early researchers (e.g., Camps and Griffis, 1982) considered the emplacement of the East Iran ophiolites as linked to the consumption of the Sistan branch of the Neotethys Ocean, with an eastward subduction vergence under the Afghan block, followed by collision between the Lut and the Afghan blokcs (Figure 9A). Tirrul et al. (1983) presented evidence in support of a northeast-dipping subduction, including the accretionary prism-forearc basin polarity, the structural vergence, the overall younging of the accretionary prism to the southwest, and the occurrence of high pressure-low temperature eclogite to blueschist facies metamorphism on the inner side of the prism. According to Tirrul et al. (1983), continued convergence of the continental blocks is reflected in a regional system of folds and transcurrent faults corresponding to an east-northeast compression.

Saccani et al. (2010) suggested that the closure of the Sistan Ocean postdated Albian and was associated with the formation of an intraoceanic arc in the course of an eastward subduction. In this model, the intraoceanic arc development had completely ceased by Maastrichtian–Paleocene times, and both MORB and suprasubduction zone (SSZ)-type lithospheric sections merged into the Birjand ophiolite and accretionary prism (Figure 9A). The subduction of the Sistan Ocean continued underneath the Afghan continental margin, as evident from the development of Maastrichtian-Paleocene intrusive and extrusive calc-alkaline rocks (Saccani et al., 2010).

Rezaei Kahkhaei et al. (2010) considered the Zargoli granite (31–33 Ma) in the Sistan suture/thrust belt (Figure 2) as the product of dehydration melting of quartzo-feldspathic metaigneous rocks or metagreywackes from

a lower crustal source, modified to some extent with subduction components, during the eastward subduction of the Sistan oceanic lithosphere under the Afghan block. The same authors also proposed an Early- to-Late Cretaceous rifting between the Lut and the Afghan cratonic blocks leading to the opening of a Late Cretaceous ocean that finally closed due to the convergence between the two blocks during the middle Eocene–Miocene times.

Mohammadi et al. (2016) suggested that the Eocene–Oligocene deformational and thermal episodes in the Sistan suture were associated with the late- and postcollisional delamination of the subcontinental mantle lithosphere under Central Iran, following an earlier eastward subduction event under the Afghan plate. The occurrence of widespread Upper Mesozoic–Cenozoic arc-related adakitic and calc-alkaline magmatism and associated ore deposits within the Lut block to the west of the Sistan suture require the operation of a west-verging subduction beneath this block which is inconsistent with the one-sided E-ENE-dipping subduction models.

5.1.2. W-dipping subduction beneath the Lut block

Zarrinkoub et al. (2012) presented a geodynamic model delineating the magmatic and tectonic history of the Sistan suture, in which the generation of MORB-type oceanic lithosphere and the Sistan Ocean resulted from rifting between the Lut and the Afghan blocks, followed by west-verging subduction under the Lut block. In this model, the East Iran ranges including the Neotethyan accretionary prism and the associated arcs, developed in Upper Cretaceous (86–71 Ma), as a result of the closure of the Sistan Ocean and subsequent Lut–Afghan collision, followed by intrusion of adakitic magmas within the Sistan suture as the initial stage of a postcollisional magmatic episode. The ocean closure is interpreted, alternatively, to have occurred in Middle Eocene (Camps and Griffis, 1982; Tirrul et al., 1983) and Late Cretaceous (Zarrinkoub et al., 2012; Angiboust et al., 2013).

Pang et al. (2013) relate the widespread Eocene–Oligocene (55–25 Ma) calc-alkaline to shoshonitic magmatic assemblages in the Lut–Sistan terrain to orogenic collapse associated with lithospheric thinning and extension at this time. The postcollisional magmatism is not related directly to subduction, the orogenic feature is probably inherited from the mantle source, presumably modified by sediment partial melt and fluid released from subducted slab during the Late Cretaceous westward subduction (Figure 9B).

Using zircon U-Pb dating of leucogabbros and whole-rock geochemical and Sr–Nd isotopic data of the Birjand ophiolite, Zarrinkoub et al. (2012) presented a geodynamic model for the Birjand ophiolites that links the development of the Sistan Ocean with early emplacement of E-MORB-, N-MORB-, and OIB-like lava flows as well as approximately 113–107 Ma MORB-type gabbros.

A lower Cretaceous opening is also supported by the occurrence of the Aptian-Albian pelagic sediments (Babazadeh and De Wever, 2004). Shafaii Moghadam and Stern (2015) presented evidence in favour of a westward intraoceanic subduction and emplacement of suprasubduction zone (SSZ)-type lava flows, gabbros, and depleted mantle harzburgites in the Late Cretaceous (100–80 Ma). The Late Cretaceous pelagic sediments, as reported by Shafaii Moghadam and Stern (2015) provide evidence in support of the survival of the Sistan Ocean by this time.

Pang et al. (2013) argued that the Sistan Ocean closure occurred in the Late Paleocene, followed by postcollisional magmatism associated with the asthenospheric upwelling during Eocene–Oligocene extensional collapse of the East Iran orogen.

5.1.3. Low-angle subduction of the Arabian plate beneath Central Iran and slab roll-back

Verdel et al. (2011) portrayed a model that relates the Late Paelocene–Oligocene magmatism in Iran, dominated by voluminous Eocene volcanism, to slab roll-back and the consequent extension in the Iranian crust following a Late-Cretaceous–Paleocene low-angle subduction along the northern margin of the Neotethyan Ocean. While the model might be applicable to magmatic assemblages in west-central and north-northwest Iran, it cannot be reconciled with the observations made in the Lut block and surroundings. The nearly N-S direction of the Lut block magmatic arc is inconsistent with that expected for a magmatic arc (NW-SE) formed during the subduction of the Arabian plate. The very long distance, >1000 km, from the Arabia suture to the northern Lut arc, further opposes this model.

In a similar scenario, Younesi et al. (2016) suggested that the Cenozoic magmatism in the Lut block occurred in a postcollisional setting and that the calc-alkaline affinity and the arc-type geochemical signature of the rocks, represented by the Mahour granitoids in the Central Lut, are indicative of partial melting of a mantle source metasomatized during the Mesozoic low-angle subduction of the Arabian plate (Neotethys oceanic crust) underneath Central Iran. The authors suggested slab retreat and postorogenic extensional collapse as a possible mechanism to trigger the magmatism.

5.2. Sabzevar zone

5.2.1. N-NNE-dipping subduction beneath the Turan block

There seems to be a consensus that the Sabzevar ophiolites formed in a nascent oceanic arc basin between the Lut block to the south and east and the Alborz zone to the north (e.g., Shojaat et al., 2003; Rossetti et al., 2010; Shafaii Moghadam et al., 2015). McCall (1997) and that considered

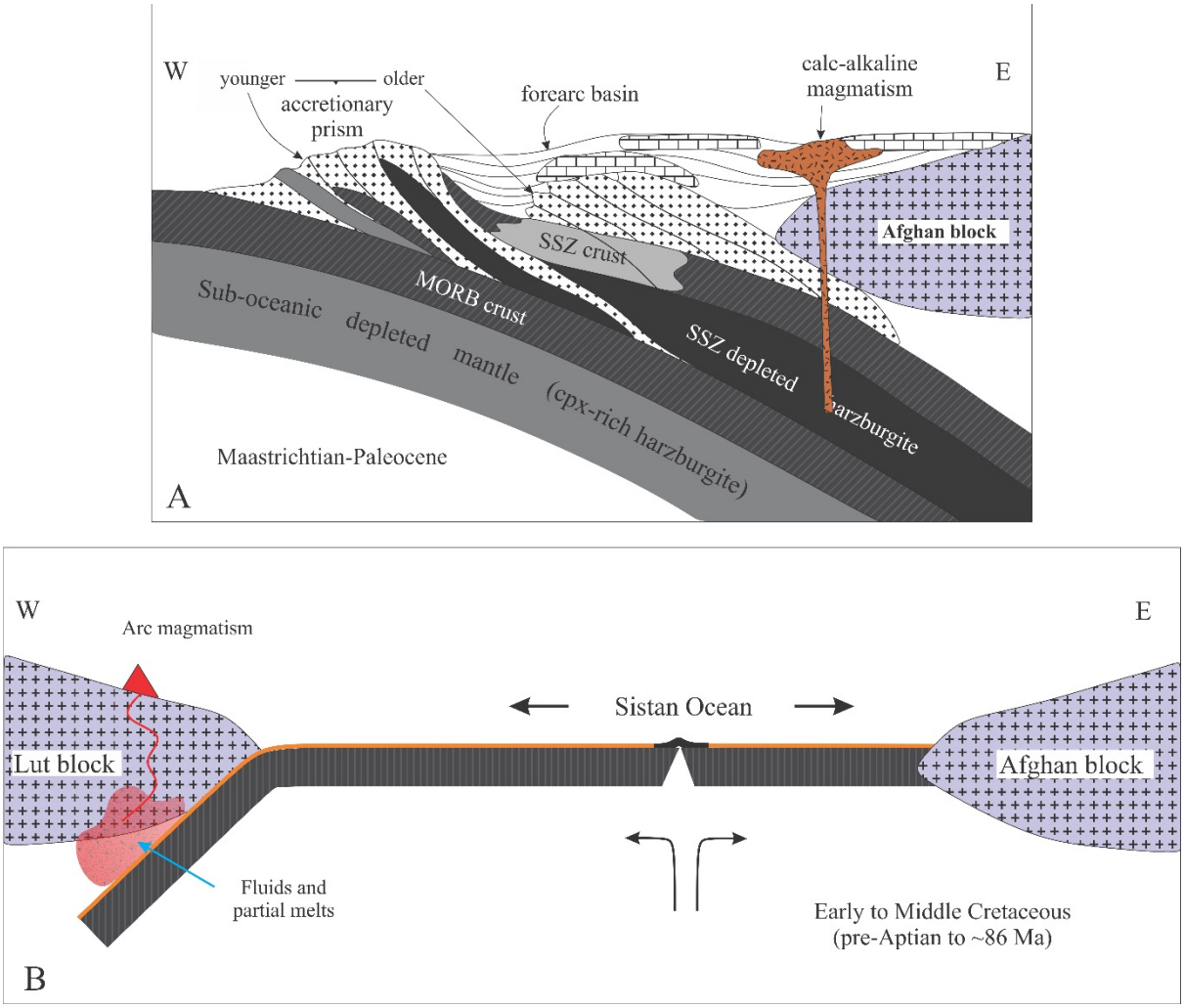

Figure 9. (A) Conceptual model showing the eastward subduction of the Sistan Ocean underneath the Afghan block and development of an accretionary prism (modified after Saccani et al., 2010). SSZ: suprasubduction zone. (B) A schematic tectonomagmatic model showing the opening of the Sistan Ocean and westward subduction underneath the Lut block, associated with upper mantle metasomatism and arc magmatism (modified after Pang et al., 2013).

the Sabzevar Ocean a subsidiary of a larger seaway in the back-arc domain of the Neotethys subduction front that included also the south Caspian Sea and the Sistan Ocean.

Shojaat et al. (2003) suggested that the emplacement of the ophiolitic complex occurred during northeast subduction of the Sabzevar Ocean in Upper Cretaceous–Early Paleocene times. The northern Sabzevar magmatic assemblages, including the Pliocene Quchan adakites of the south Kopeh-Dagh Ranges (Figures 1 and 2) are considered to be the products of partial melting of a subducted eclogitic slab after cessation of the north-dipping subduction of the Sabzevar oceanic crust under the Turan block (Ghasemi et al., 2010).

Shabanian et al. (2012) proposed a model for the Quchan adakitic rocks involving postcollisional melting of the oceanic slab and/or mafic lower crust, triggered by asthenospheric rise associated with slab break-off or intramantle delamination. Jamshidi et al. (2018) interpreted the Quchan adakites as products of partial melts derived from a garnet-amphibolite source that originated from metamorphism of the Sabzevar subducted oceanic slab.

Shojaat et al. (2003) suggested a model whereby the Sabzevar orogenic system developed during the north-dipping subduction of the Sabzevar Ocean underneath the Turan block. The structural evidence such as the occurrence of NNE–dipping thrust faults and associated folds vergence in SOZ, further supports a northward subduction (Bagheri and Stampfli, 2008).

Using in situ zircon and titanite U–Pb dates for the felsic melt segregations in the Sabzevar granulites, Rossetti et al. (2010) suggested an uppermost Lower Cretaceous

age for the peak of metamorphism in the Sabzevar ophiolitic assemblage. The authors argued for a scenario for the development of the Sabzevar granulites involving slab melting in the course of northeastward subduction of an intra-Cimmerian oceanic crust.

Upper Cretaceous to Lower Eocene granitoids with zircon U–Pb ages of ca. 97 Ma and 68–49 Ma (Shafaii Moghadam et al., 2016) are abundant in the Arghash area to the southeast of the Sabzevar ophiolites (Figure 2). Younger adakitic and calc-alkaline plutonic and volcanic rocks (ca. 45–30 Ma; Shafaii Moghadam et al., 2016) are also widespread in the Arghash area.

Omrani et al. (2018) linked the granulite and blueschist rocks in the Sabzevar zone to the north-dipping subduction of the Sabzevar oceanic crust and subsequent closure during Lower Eocene between the central Iranian microcontinent and the Turan block. The same authors presented tectonomagmatic model that indicates that the mafic granulites were formed in a suprasubduction zone while the blueschists were generated during the subduction (Figure 10A). The 101-75 Ma magmatic rocks of southern Sabzevar (CSI) with moderate Mg# and initial $^{87}Sr/^{86}Sr$ and εNd (t) ranging from 0.70411 to 0.70628 and +5.8 to +7.4, respectively, are explained by partial melting of a MORB-type slab/depleted-mantle wedge source during the northward subduction of the Sabzevar oceanic slab under the Turan block in Late Cretaceous time (Kazemi et al., 2019).

5.2.2. S- SSW-dipping subduction beneath the Lut block

Berberian and King (1981) interpreted the Sabzevar ophiolites as belonging to a seaway that enclosed the central east Iran microcontinent (CEIM). Shafaii Moghadam and Stern (2015) reported TIMS zircon U-Pb ages of 77.8–99.9 Ma. for the plagiogranites in the Sabzevar ophiolites, and suggested a Late Campanian to Early Maastrichtian age for the pelagic sediments covering the ophiolites. The ophiolitic units developed in an arc-back arc basin associated with an ocean that opened between the Lut block to the south and the Alborz belt to the north in mid-Cretaceous time (Shafaii Moghadam and Stern, 2015).

From the chronology of felsic segregates (zircon and titanite U-Pb ages of 107.4 ± 2.4 and 105.9 ± 2.3 Ma) in the Sabzevar mafic granulites, Rossetti et al. (2010) suggested that the south-dipping intraoceanic subduction beneath the Lut block began prior to Albian (Figure 10B).

Mahdavi et al. (2016) suggested that the Gazu, Kajeh, and Bajestan intrusives in northern Lut block define a NE-SW trend and developed in a subduction setting. The authors argued that the Sabzevar basin developed during a back-arc extension event in the Early Cretaceous and that the oceanic crust began to subduct under the CEIM during the middle Cretaceous. According to Stampfli and Borel (2004), the Sabzevar back-arc basin was closed during the Late Cretaceous to Eocene, leading to the emplacement of Late Cretaceous to Paleocene ophiolite melanges.

6. Discussion

A review and synthesis of the available geological, geochemical, geochronological, and structural evidence from the Sabzevar ophiolite zone and the Lut block allows us to propose a two-sided asymmetric subduction for the Upper Mesozoic–Cenozoic magmatism in the Lut block.

6.1. Sistan Ocean

The timing of the Sistan Ocean closure and development of the suture is not well-constrained. Camps and Griffis (1982) and Tirrul et al. (1983) provided structural and stratigraphic evidence such as the deformation of Eocene deposits and the increase of clastic coarse-grained sediments at this time and suggested that the Ocean closure occurred in the Middle Eocene. Based on paleogeographic reconstruction, Sengör and Natalin (1996) proposed a younger Oligocene–Middle Miocene age for the closure of the Ocean in East Iran, between the Afghan and the Lut blocks.

Zarrinkoub et al. (2012) presented evidence that rifting across the Sistan Ocean in Lower Cretaceous was followed by early emplacement of N-MORB-, E-MORB-, and OIB-like lava flows as well as Albian MORB-type gabbros. This is further supported by the occurrence of gabbroic rocks, Aptian–Albian pelagic sediments and radiolarian remains with the volcanic materials (Babazadeh and de Wever, 2004) (Figure 11A).

The occurrence of high-pressure/low-temperature metamorphic rocks and associated amphibolites in the Birjand ophiolites with Rb–Sr ages of ~84-87 Ma suggests that subduction of the Sistan Ocean and the accompanying metamorphism was active in the Upper Cretaceous (Bröcker et al., 2013). The survival of the Sistan Ocean by Late Cretaceous is supported by pelagic sediments of this time (Babazadeh and de Wever, 2004). Considering a Late Cretaceous time for the ophiolite emplacement, and the occurrence of extensive postcollisional Eocene–Oligocene magmatism in the Lut block, the Late Cretaceous–Paleocene appears to be the preferred time for the Sistan ocean closure.

Arc-type assemblages in the Lut block, Sistan suture zone, and Afghan block consisting of calc-alkaline to shoshonitic and adakitic volcanic–plutonic rocks developed during the latest Cretaceous to Middle Paleocene. The Bibi-Maryam high-silica tonalitic intrusives to the east of the Sistan suture zone (Figures 2 and 3) dated at 71.5 ± 0.6 Ma (Maestrichtian) (zircon U-Pb, Zarrinkoub et al., 2011) are explained by partial melting of the northeast-dipping Sistan oceanic crust (Zarrinkoub et al., 2010). The Mahirud volcanic–plutonic suite (Figure 2) within the Afghan block, developed in an island arc setting during the Late Cretaceous (Keshtgar et al., 2019), provides further

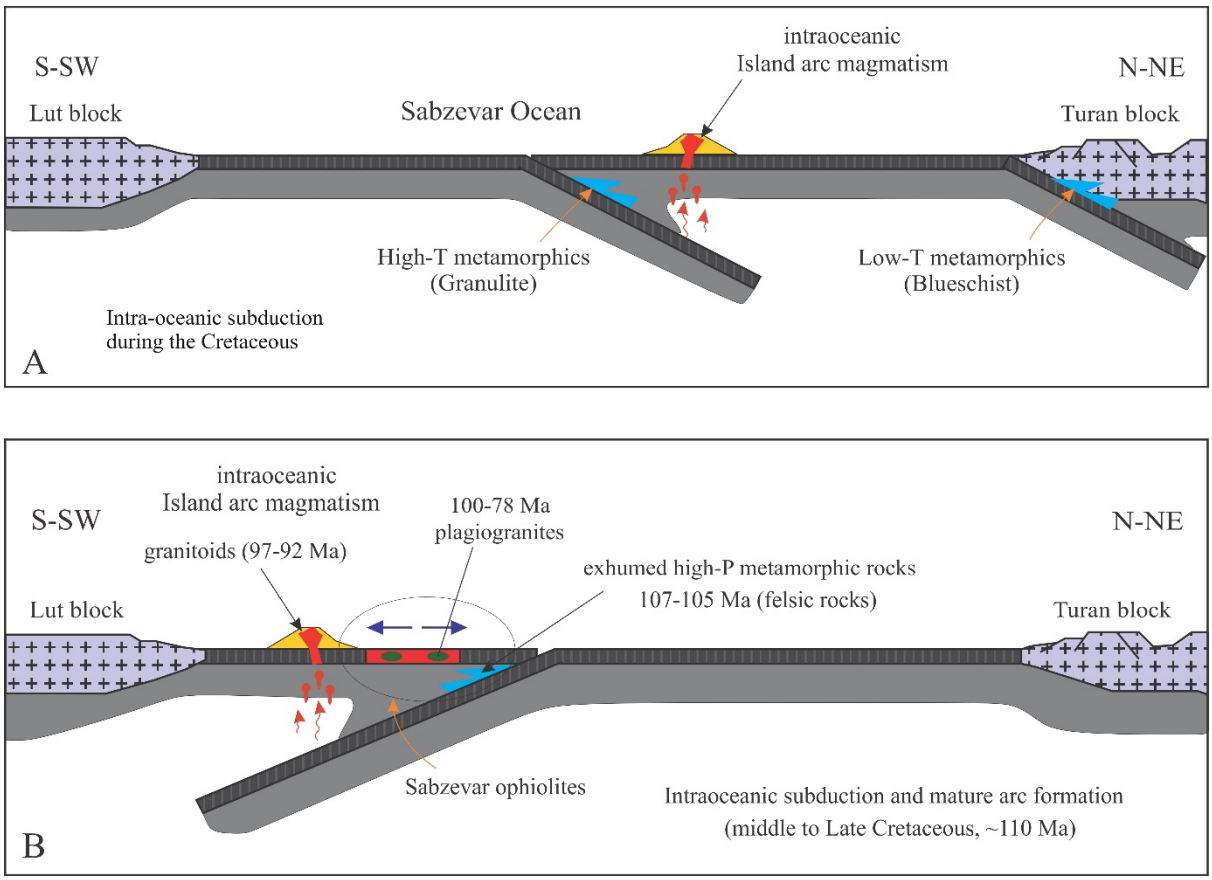

Figure 10. Cartoons showing the evolution of the Sabzevar Ocean. (A) A tectonomagmatic model showing the N-NNE-dipping subduction of the Sabzevar Neotethyan oceanic lithosphere under the Turan block and an intraoceanic subduction during the Cretaceous (modified after Omrani et al., 2018). (B) A model for southward intraoceanic subduction of the Sabzevar oceanic lithosphere under the Lut block in the mid-Cretaceous. The high-P metamorphic rocks were exhumed during the formation of a mature arc in the Late Cretaceous (modified after Shafaii Moghadam and Stern, 2015).

support in favour of an eastward subduction at this time.

On the opposite side, the occurrence of Bazman granitoid complex (83.07 ± 0.30 to 72.50 ± 0.1 Ma) in the southern Lut block and west of the Sistan suture (Figure 1) can be attributed to a west-dipping subduction. The simultaneous occurrence of the two subduction-related magmatic assemblages to the west and east of the Sistan suture in Late Cretaceous provides evidence in support of a double-verging subduction beneath both the Lut and the Afghan blocks.

Paleocene was a period of transition, with no major magmatism, from the Late Cretaceous oceanic consumption and ophiolite emplacement to the Eocene–Oligocene continental arc magmatism. The Paleocene gap can be linked to a period of progressive continental collision followed by the syn- and postcollisional relaxation/extension and associated high-K calc-alkaline magmatism in an extensional geodynamic regime peaking at Middle Eocene.

An island arc setting for the middle Eocene high-K calc-alkaline to shoshonitic shallow intrusions in Maherabad-Khopic, as proposed by Malekzadeh Shafaroudi et al. (2010) is inconsistent with the geological evolution of the Lut block in Paleogene with widespread Eocene postcollisional magmatism as discussed earlier.

The lower Oligocene (approximately 33 Ma) Dehsalm and Chah-shaljami granitoids in the central Lut block formed in a mature continental arc developed with the convergence of the Afghan and the Lut blocks.

The relatively high Mg# for the Dehsalm, Chah-shaljami, and Kashmar intrusive bodies suggest the involvement of a mantle source in the production of the parent magmas. Arc magmas formed from partial melting of a subducting oceanic slab or of lower crustal mafic rocks commonly have lower Mg#, <40, irrespective of the degree of partial melting (Rapp and Watson, 1995).

The geochemical features of the Dehsalm and Chah-shaljami intrusions, as presented in Section 3.2.2, are

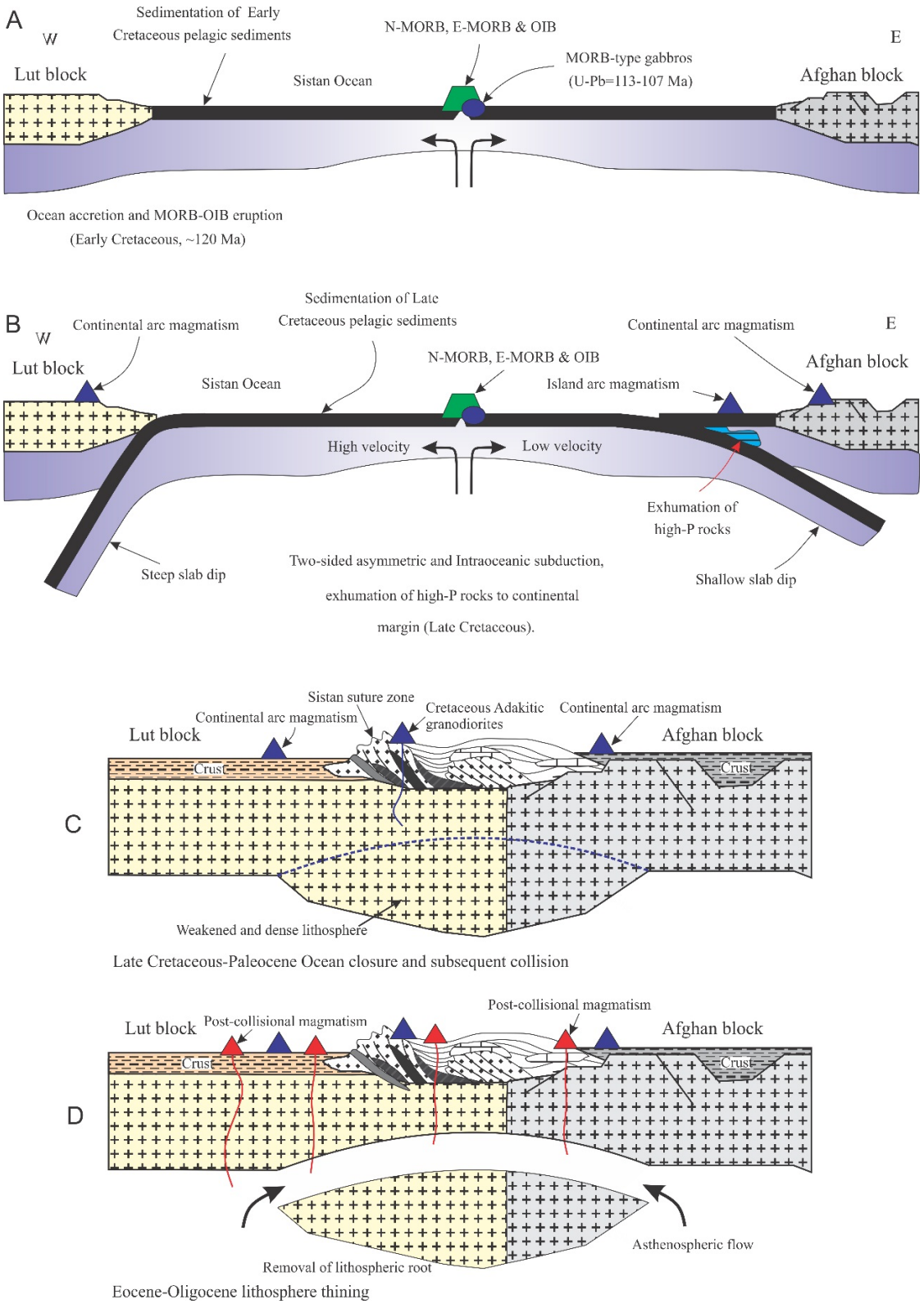

Figure 11. (A,B) Cartoons showing a model for an Early-to-Late Cretaceous two-sided asymmetric subduction for the Sistan Ocean (A) and development of magmatic arcs (B). (C,D) Paleogene tectonomagmatic sketch illustrating the collision of the Lut and Afghan blocks, development of the Sistan suture and of a thickened and dense lithosphere (C), followed by the widespread Eocene–Oligocene magmatism, as a result of lithospheric delamination and subsequent asthenospheric upwelling (D).

consistent with partial melting of a mantle peridotite source metasomatized and modified by subduction components (c.f. Prouteau et al., 2001). The Sr and Nd isotopic compositions for the intrusions are very similar to those of normal island-arc basalts (Figure 8) and can be explained by derivation of the magma in a mantle wedge followed by magmatic differentiation (c.f. White and Patchett, 1984).

The elemental and isotopic geochemical characteristics for the CAS, CLB, NLB, and SOZ igneous rocks differ from the so-called C-type adakites that are known to be the products of fluid-absent partial melting of K-rich (meta-) basaltic, dioritic, or tonalitic rocks at the base of overthickened crust and under elevated geothermal gradients (Xiao and Clemens, 2007).

The C-type adakites, as reported by Xiao and Clemens (2007) are distinguished by high SiO_2 contents (>67 wt%) and moderate Mg# (40–46), and are moderately peraluminou (A/CNK: 1.02–1.06). Moreover, in contrast to CAS, SOZ, NLB, and CLB igneous rocks with low ($^{87}Sr/^{86}Sr$)i ratios and positive εNdi values (Figure 8), the initial 87Sr/86Sr > 0.708 and εNd < −13 for C-type adakites indicate the involvement of crustal materials in their formation and evolution (Xiao and Clemens 2007; Deng et al., 2018). The geochemical features of rocks in the CLB are thus consistent with a postcollisional setting, implying that the parental melts were generated in a suprasubduction mantle wedge

The geological evidence presented and discussed above and the configuration of various components from the Lut block and the Sistan suture allows us to propose a two-sided asymmetric subduction that involves both W-SW- and E-NE-dipping subductions, respectively under the Lut and Afghan blocks, with different rates of consumption of oceanic lithosphere.

Besides W-dipping subduction underneath the Lut block, which is testified by the Upper Mesozoic–Cenozoic subduction-modified slab-/mantle-derived magmas as discussed above, several features suggest that the Ocean closure was also associated with eastward subduction. These include the accretionary prism-forearc basin polarity, the structural vergence and general younging of the accretionary prism to the southwest, and the occurrence of the relatively high pressure-low temperature metamorphic rocks on the inner portions of the prism (Tirrul et al., 1983).

The kinematic estimates of subduction zones and the mechanism of the slab hinge such as the subduction rate, the velocity of the subduction hinge, and the velocity of the lower plate, indicate that the sinking velocity of the E- or NE-dipping slabs is slower than that of the W-dipping slabs (Doglioni et al., 2009). The west-verging subducting slabs would thus be completely consumed before the E- or NE-verging slabs, implying that the ocean closure occurs to the east or northeast. This would lead to the development of structures that display features in favour of one-sided subduction as previously reported between the Lut and the Afghan blocks.

Bonnet et al. (2018) provided evidence that the greenschist recrystallization of the siliciclastic-matrix complex hosting oceanic blocks in the Sistan suture could have developed during shallow subduction at depths between 10 and 20 km. The finding is in good agreement with the geodynamic model proposed by Doglioni et al. (2009) and also with our double-verging subduction model for the East Iran in which a low angle subduction is considered beneath the Afghan block to the east.

The thick (up to 2000 m) Cenozoic subduction-related volcanic and subvolcanic rocks covering half of the Lut block can be explained by a greater rate of subduction associated with a W-directed slab (e.g., Doglioni et al., 2009). The occurrence of arc type igneous rocks both to the east, represented by the Zargoli granite (Rezaei Kahkhaei et al., 2010) and Mahirud volcanic–plutonic suite (Keshtgar et al., 2019), and to the west, represented by the Bazman and CLB granitoids, is consistent with a two-sided asymmetric subduction model.

An island arc setting for the Upper Eocene Maherabad-Khopic intrusive bodies, as proposed by Malekzadeh Shafaroudi et al. (2015), can be revised in the context of a double subduction model. In such scenario, the postcollisional Eocene–Oligocene magmatic rocks in the Lut block were formed as a result of the extensional collapse of East Iran due to the removal of the lithospheric root and the subsequent asthenospheric upwelling (Figure 11B).

6.2. Sabzevar Ocean

The stratigraphic, geochemical, and geochronological investigations on the Sabzevar ophiolites suggest that the Ocean was opened between the Turan block to the north and the Lut block to the south since at least the mid-Cretaceous period (Rossetti et al., 2010; Agard et al., 2011). Similarly, Shafaii Moghadam and Stern (2015) presented evidence that the intraoceanic subduction in the Sabzevar oceanic basin and development of the Sabzevar SSZ-related magmas began prior to Albian (100–113 Ma) and that the continued subduction created a magmatic arc to the south of the Sabzevar ophiolites (Figure 12).

On the opposite side, to the north of the Sabzevar suture, the Cretaceous magmatism in Arghash (Figure 2) represented by a magmatic arc developed across the southern border of the Alborz zone, can be explained by northeast-dipping subduction of the Sabzevar Ocean. Besides that, Kazemi et al. (2019) linked the Late Cretaceous igneous rocks on the southern edge of the Sabzevar basin to the north-verging subduction of the Sabzevar oceanic slab under the Turan block in Late Cretaceous time.

It is assumed that the Early Eocene is the minimum age for subduction of the oceanic crust. Accordingly, the postophiolitic arcs developed shortly after the final collision and closure of the Sabzevar basin.

In a more recent study on the metamorphic history of the Sabzevar suture using Rb–Sr and U–Pb chronology data on blueschist and amphibolite facies rocks, Bröcker et al. (2021) proposed a geodynamic model involving Cretaceous to Eocene northward-directed subduction of the Neotethys Ocean under the Turan block. The subduction-related magmatic rocks in the Sabzevar zone are thus bracketed in time between Cretaceous and Eocene times. The occurrence of Eocene subduction-related magmatic suites both to the north and south of the Sabzevar ophiolites, with greater exposures in the south is rather consistent with a two-sided asymmetric subduction.

The Middle Eocene Najmabad adakitic granitoids to the south of the Dorouneh fault in the northern Lut block is linked to the subduction of the Sistan Ocean under the Lut block (Moradi Noghondar et al., 2012). In addition to the proximity to the southern Sabzevar volcanic arc, the NLB granitoids possess isotopic and geochemical attributes similar to those of the Sabzevar adakitic lava flows, but different from those of the central Lut block (CLB). The inference is that the NLB igneous suite formed during a S-SW-dipping subduction of the Sabzevar Ocean, and not the westward subduction of the Sistan Ocean, under the Lut block.

Similar to the tectonomagmatic model of the eastern Lut block and the Sistan suture, a two-sided N-NE- and S-SW-dipping asymmetric subduction beneath both the Turan block and the Lut block can be envisaged for the Sabzevar suture and the northern Lut block (Figure 12). A two-sided asymmetric subduction model would explain the occurrence of asymmetrically distributed Cretaceous–Eocene magmatic rocks to the north and south of the Sabzevar ophiolites. This model further explains why the Eocene granitoids in the northern Lut block possess isotopic and geochemical attributes similar to those of the south Sabzevar ophiolite but different from those of the central Lut block. The occurrence of high-pressure-low temperature metamorphic rocks within both Sabzevar and Sistan sutures can be explained by east-northeast dipping subduction beneath both Turan and Afghan blocks.

7. Conclusion

The one-sided subduction models, as previously proposed for the Sistan and Sabzevar Oceans, fail to explain the regional configuration and spatial-temporal distribution of the Upper Mesozoic–Cenozoic magmatic assemblages in the Lut block and in the Sabzevar zone. The data presented and discussed in this work are in favour of a two-sided asymmetric subduction model for both Sistan and Sabzevar Oceans.

The geochemical attributes of the Late Cretaceous magmatic rocks in the southern, central, and northern Lut block, eastern Sistan suture, and in the Sabzevar zone are indicative of a subduction-related volcanic arc setting. The Eocene–Oligocene magmatic rocks in the central Lut block postdate the closure of the Sistan Ocean and display an orogenic signature.

The Late Cretaceous–Eocene magmatic rocks in the northern Lut block developed in response to the S-SW-dipping subduction of the Sabzevar Ocean, not the Sistan Ocean, under the Lut block. The isotope geochemistry and the TDM data indicate similarities in the source and evolution of the parent magmas between the Sabzevar and the northern Lut block Eocene volcanic and intrusive rocks. The two suites of rocks developed in the same tectonomagmatic setting associated with the double-

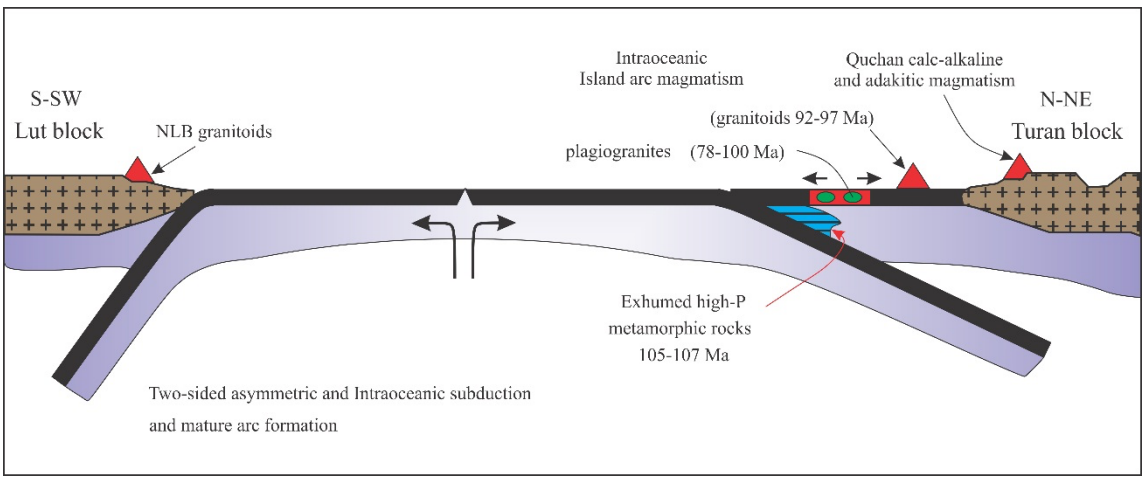

Figure 12. Proposed model for the tectonomagmatic setting of the Sabzevar Ocean and associated arcs, involving a two-sided asymmetric subduction. NLB: northern Lut block.

verging subduction beneath both the Lut and the Turan blocks.

Acknowledgements
This work was supported by a Payame Noor University grant (7/47416/D, 2018) to RA and a Shahid Beheshti University grant (2455/600/D) to SA. The authors would like to warmly thank the editor Dr Yener Eyuboglu and the reviewer Dr Ze Liu for insightful reviews, comments, and suggestions that greatly improved the manuscript. The manuscript also benefitted from comments by one anonymous reviewer.

References

Agard P, Omrani J, Jolivet L, Whitechurch H, Vrielynck B et al. (2011) Zagros orogeny: A subduction-dominated process: Geological Magazine 148: 692–725.

Aguillón-Robles A, Caimus T, Bellon H, Maury C, Cotton J et al. (2001). Late Miocene adakites and Nb enriched basalts from Vizcaino Peninsula, Mexico: indicators of East Pacific Rise subduction below southern Baja California. Geology 29: 531–534.

Ahmadi-Rouhani R, Karimpour MH, Rahimi B, Malekzadeh Shafaroudi A, Urs Klötzli U et al. (2017). Petrology, geochronology, geochemistry and petrogenesis of Bajestan granitoids, North of Ferdows, Khorasan Razavi Province. Journal of Economic Geology 8: 525-552 (in Persian with English abstract).

Alirezaei S, Hassanzadeh J (2012). Geochemistry and zircon geochronology of the Permian A-type Hasanrobat granite, Sanandaj–Sirjan belt: A new record of the Gondwana break-up in Iran. Lithos 151: 122–134.

Almasi A, Karimpour MH, Arjmandzadeh R, Santos JF, Ebrahimi Nasrabadi K (2019). Zircon U-Pb geochronology, geochemistry, Sr-Nd isotopic compositions and tectonomagmatic implications of Nay (NE Iran) post-collisional intrusives in Sabzevar zone. Turkish Journal of Earth Sciences 28: 372-397.

Angiboust S, Agard P, De Hoog JCM, Omrani J, Plunder A (2013). Insights on deep, accretionary subduction processes from the Sistan ophiolitic mélange (Eastern Iran). Lithos 156–159: 139-158.

Arjmandzadeh R, Karimpour MH, Mazaheri SA, Santos JF, Medina JM et al. (2011). Sr/Nd isotope geochemistry and petrogenesis of the Chah-shaljami granitoids (Lut Block, Eastern Iran). Journal of Asian Earth Sciences 41: 283-296.

Arjmandzadeh R, Santos JF (2014). Sr-Nd isotope geochemistry and tectonomagmatic setting of the Dehsalm Cu-Mo porphyry mineralizing intrusives from Lut Block, eastern Iran. International Journal of Earth Sciences 103: 123-140.

Arvin M, Pan Y, Dargahi S, Malekizadeh A, Babaei A (2007). Petrochemistry of the Siah-Kuh granitoid stock southwest of Kerman, Iran: Implications for initiation of Neotethys subduction. Journal of Asian Earth Sciences 30: 474-489.

Babazadeh SA, De Wever P (2004). Radiolarian Cretaceous age of Soulabest radiolarites in ophiolite suite of eastern Iran. Bulletin de la Société Géologique de France175: 121-129.

Bagheri S, Stampfli GM (2008). The Anarak, Jandaq, and Posht-e-Badam metamorphic complexes in central Iran: new geological data, relationships and tectonic implications. Tectonophysics 451: 123–155.

Berberian M, King GCP (1981). Towards a paleogeography and tectonic evolution of Iran. Canadian Journal of Earth Sciences 18: 210-265.

Beydokhti RM, Karimpour MH, Mazaheri SA, Santos JF, Klötzli U (2015). U-Pb zircon geochronology, Sr-Nd geochemistry, petrogenesis and tectonic setting of Mahour granitoid rocks (Lut Block, Eastern Iran). Journal of Asian Earth Sciences 111: 192–205.

Bonnet G, Agard P, Angiboust S, Monié P, Jentzer M et al. (2018). Tectonic slicing and mixing processes along the subduction interface: The Sistan example (Eastern Iran). Lithos 310–311: 269–287.

Bröcker M, Fotoohi Rad G, Burgess R, Theunissen S, Paderin I et al. (2013). New age constraints for the geodynamic evolution of the Sistan Suture Zone, eastern Iran. Lithos 170: 17-34.

Bröcker M, Omrani H, Berndt J, Moslempour ME (2021). Unraveling metamorphic ages of suture zone rocks from the Sabzevar and Makran areas (Iran): Robust age constraints for the larger Arabia–Eurasian collision zone. Journal of Metamorphic Geology 00: 1–31.

Camp VE, Griffis RJ (1982). Character, genesis and tectonic setting of igneous rocks in the Sistan suture zone, eastern Iran. Lithos 15: 221–239.

Castillo PR (2006). An overview of adakite petrogenesis. Chinese Science Bulletin 51: 258–268.

Castillo PR (2012). Adakite petrogenesis. Lithos 134–135: 304-316.

Chappell BW, White AJR (1992). I- and S-type granites in the Lachlan fold belt. Transactions of the Royal Society of Edinburgh Earth Sciences 83: 1–26.

Chappell BW, White AJR (1974). Two contrasting granite types. Pacific Geology 8: 173–174.

Cherniak DJ, Dimanov A (2010). Diffusion in pyroxene, mica and amphibole. Reviews in Mineralogy and Geochemistry 72: 641–690.

Conticelli S, Guarnieri L, Farinelli A, Mattei M, Avanzinelli R et al. (2009). Trace elements and Sr–Nd–Pb isotopes of K-rich, shoshonitic, and calc-alkaline magmatism of the Western Mediterranean Region: Genesis of ultrapotassic to calc-alkaline magmatic associations in a post-collisional geodynamic setting. Lithos 107: 68-92.

Davoudzadeh M, Weber-Diefenbach K (1987). Contribution to the Paleogeography, Stratigraphy and Tectonics of the Upper Paleozoic in Iran. Neue. Neues Jahrbuch für Geologie und Paläontologie 175: 121–146.

Defant MJ, Drummond MS (1990). Derivation of Some Modern Arc Magmas by Melting of Young Subducted Lithosphere. Nature 347: 662–665.

Defant MJ, Jackson TE, Drummond MS, Deboer JZ, Bellon H et al. (1992). The Geochemistry of young volcanism throughout western Panama and southeastern Costa–Rica – an overview. Journal of the Geological Society of London 149: 569–579.

Deng C, Sun G, Sun D, Huang H, Jhang J et al. (2018). Origin of C type adakite magmas in the NE Xing'an block, NE China and tectonic implication. Acta Geochimica 37: 281–294.

DePaolo DJ (1981). Trace-Element and Isotopic Effects of Combined Wallrock Assimilation and Fractional Crystallization. Earth and Planetary Science Letters 53: 189–202.

DePaolo DJ, Wasserburg GJ (1976). Inferences about magma sources and mantle structure from variations of 143Nd/144Nd. Geophysical Research Letters 3: 743–6.

DePaolo DJ, Wasserburg GJ (1979). Petrogenetic mixing models and Nd–Sr isotopic patterns. Geochimica et Cosmochimica Acta 43: 615–27.

Doglioni C, Tonarini S, Innocenti F (2009). Mantle wedge asymmetries and geochemical signatures along W- and E–NE-directed subduction zones. Lithos 113: 179–189.

Esmaeily D, Nédélecb A, Valizadeha MV, Moorec F, Cottend J (2005). Petrology of the Jurassic Shah-Kuh granite (eastern Iran), with reference to tin mineralization. Journal of Asian Earth Sciences 25: 961–980.

Eyuboglu Y, Santosh M, Chung SL (2011). Crystal fractionation of adakitic magmas in the crust–mantle transition zone: Petrology, geochemistry and U–Pb zircon chronology of the Seme adakites, eastern Pontides, NE Turkey. Lithos 121: 151–166.

Gardideh S, Ghasemi H, Sadeghian M (2018). U-Pb age dating on zircon crystals, Sr-Nd isotope ratios and geochemistry of Neogene adakitic domes of Quchan-Esfarayen magmatic belt, NE Iran. Iranian Journal of Crystallography and Mineralogy 26: 455-478 (in Persian with English abstract).

Geological Survey of Iran (1992a). 1:250,000 Geological quadrangle map of Iran, No. K8: Birjand: Tehran, Geol. Surv. Iran. 1 map sheet.

Geological Survey of Iran (1992b). 1:250,000 Geological quadrangle map of Iran, No. K9: Dehsalm (Chah Vak): Tehran, Geol. Surv. Iran. 1 map sheet.

Ghasemi H, Sadeghian M, Khan Alizadeh AR, Tanha A (2010). Petrology, geochemistry and radiometric ages of high silica adakitic domes of Neogene continental arc, south of Quchan. Iranian Journal of Crystallography and Mineralogy 18: 347–370 (in Persian with English abstract).

Ghodsi M, Boomeri M, Bagheri S, Ishiyama D, Corfu F (2016). Geochemistry, zircon U-Pb age, and tectonic constraints on the Bazman granitoid complex, southeast Iran. Turkish Journal of Earth Sciences 25: 311-340.

Glennie KW (2000). Cretaceous tectonic evolution of Arabia's eastern plate margin, a tale of two oceans. Society for Sedimentary Geology 69: 9–20.

Gust DA, Arculus RJ, Kersting AB (1997). Aspects of magma sources and processes in the Honshu arc. Canadian Mineralogist 35: 347–365.

Hassanzadeh J, Wernicke BP (2016). The Neotethyan Sanandaj-Sirjan zone of Iran as an archetype for passive margin-arc transitions. Tectonics 35: 586-621.

Horton R, Herweijer, C, Rosenzweig, C, Liu, J.P, Gornitz, V et al. (2008). Sea level rise projections for current generation CGCMs based on the semi-empirical method. Geophysical Research Letters 35: L02715, doi: 10.1029/2007GL032486.

Hosseini MR, Hassanzadeh J, Alirezaei S, Sun W, Li C-Y (2017). Age revision of the Neotethyan arc migration into the southeast Urumieh-Dokhtar belt of Iran: Geochemistry and U–Pb zircon geochronology. Lithos 284-285: 296-309.

Ionov DA, Hofmann AW (1995) Na-Ta-rich mantle amphiboles and micas: implications for subduction-related metasomatic trace element fractionations. Earth and Planetary Science Letters 131:341–356.

Irvine TN, Baragar WRA (1971). A guide to the chemical classification of the common volcanic rocks. Canadian Journal of Earth Sciences 8: 523-548.

Jamshidi K, Ghasemi H, Miao L, Sadeghian M (2018). Adakite magmatism within the Sabzevar ophiolite zone, NE Iran: U-Pb geochronology and Sr-Nd isotopic evidences. Geopersia 8: 111-130.

Jentzer M, Whitechurch H, Agard P, Ulrich M, Caron B et al. (2020). Late Cretaceous calc-alkaline and adakitic magmatism in the Sistan suture zone (Eastern Iran): implications for subduction polarity and regional tectonics. Journal of Asian Earth Sciences 204: 104588.

Karimpour MH, Stern CR, Farmer L, Saadat S, Malekzadeh Shafaroudi A (2011). Review of age, Rb-Sr geochemistry and petrogenesis of Jurassic to Quaternary igneous rocks in Lut Block, Eastern Iran. Geopersia 1: 19-36.

Karimpour MH, Malekzadeh Shafaroudi A, Moradi Noghondar M, Farmer L, Stern CR (2014). Geology, mineralization, Rb-Sr & Sm-Nd geochemistry, and U–Pb zircon geochronology of Kalateh-Ahani Cretaceous intrusive rocks, southeast Gonabad. Journal of Economic Geology 5: 267-290 (in Persian with English abstract).

Kay SM, Ramos VA, Marquez M (1993). Evidence in Cerro Pampa volcanic rocks of slab melting prior to ridge trench collision in southern South America. Journal of Geology 101: 703–714.

Kazemi Z, Ghasemi H, Tilhac R, Griffin W, Shafaii Moghadam H et al. (2019). Late Cretaceous subduction-related magmatism on the southern edge of Sabzevar basin, NE Iran. Journal of the Geological Society of London 176: 530-552.

Keshtgar Sh, Bagheri S, Boomeri M (2019). Tectonic setting of Mahirud Volcano-plutonic Complex: Different insight into the geodynamic history of East Iran. Geosciences Scientific Quarterly Journal 29: 131-144 (in Persian with English abstract).

Le Maitre RW (2002). Igneous Rocks: A Classification and Glossary of Terms. Recommendations of the International Union of Geological Sciences Subcommission on the Systematics of Igneous Rocks. Cambridge University Press, Cambridge UK.

Mahdavi A, Karimpour MH, Mao JW, Shahri MRH, Malekzadeh Shafaroudi A et al. (2016). Zircon U-Pb geochronology, Hf isotopes and geochemistry of intrusive rocks in the gazu copper deposit, Iran: Petrogenesis and geological implications. Ore Geology Review 72: 818–837.

Malekzadeh Shafaroudi A, Karimpour MH, Mazaheri SA (2010). Rb-Sr and Sm-Nd isotopic compositions and petrogenesis of syn-mineralization intrusive rocks of gold-rich porphyry copper Maher-abad prospect area (north of Hanich), east of Iran. Iranian Journal of Crystallography and Mineralogy 18: 15-32 (in Persian with English abstract).

Malekzadeh Shafaroudi A, Karimpour MH, Stern CR (2015). The Khopik porphyry copper-gold prospect, Lut Block, Eastern Iran: geology, alteration, mineralization, fluid inclusion, and oxygen isotope studies. Ore Geology Review 65: 522–544.

Maniar PD, Piccoli PM (1989). Tectonic Discrimination of Granitoids. Geological Society of America 101.

Martin H (1999). The adakitic magmas: modern analogues of Archaean granitoids. Lithos 46: 411–429.

Mason DR, McDonald JA (1978). Intrusive rocks and porphyry copper occurrences of the Papua New Guinea-Solomon Islands region. Economic Geology 73: 857–877.

Mattei M, Cifelli, F, Muttoni G, Zanchi A, Fabrizio Berra F, et al. (2012). Neogene block rotation in central Iran: Evidence from paleomagnetic data. Geological Society of America Bulletin 124: 943–956.

McCall GJH (1997). The geotectonic history of the Makran and adjacent area of Southern Iran: Journal of Asian Earth Sciences 15: 517–531.

Moghadam HS, Stern RJ (2011). Geodynamic evolution of Upper Cretaceous Zagros ophiolites: formation of oceanic lithosphere above a nascent subduction zone. Geological Magazine 148: 762–801.

Mohammadi A, Burg J-P, Bouilhol P, Ruh J (2016). U–Pb geochronology and geochemistry of Zahedan and Shah Kuh plutons, southeast Iran: Implication for closure of the South Sistan suture zone. Lithos 248-251: 293–308.

Moix P, Beccaletto L, Kozur HW, Hochard C, Rosselet F, Stampfli GM (2008). A new classification of the Turkish terranes and sutures and its implication for the paleotectonic history of the region. Tectonophysics 451: 7–39.

Moradi Noghondar M, Karimpour MH, Farmer L, Stern CR (2011). Sr-Nd isotopic characteristic, U-Pb zircon geochronology, and petrogenesis of Najmabad Granodiorite batholith, Eastern Iran. Journal of Economic Geology 3: 127-145 (in Persian with English abstract).

Moradi Noghondar M, Karimpour MH, Malekzadeh Shafaroudi A, Farmer L, Stern CR (2012). Geochemistry, zircon U-Pb geochronology and Rb-Sr & Sm-Nd isotopes of Najmabad monzonitic rocks south of Gonabad. Petrology 3: 77-96 (in Persian with English abstract).

Maurizot P, Fauvelet E, Eftekhar-Nezhad J (1990). Explanatory text of the Gazik quadrangle map 1:250,000. GSI.

Moyen J.-F (2009). High Sr/Y and La/Yb ratios: the meaning of the "adakitic signature". Lithos 112: 556-574.

Muller D, Groves DI (1997). Potassic igneuos rocks and associated gold -copper mineralization, sec. updated. Springer-Verlag, 242pp.

Müntener O, Pettke T, Desmurs L, Meier M, Schaltegger U (2004). Refertilization of mantle peridotite in embryonic ocean basins: trace element and Nd isotopic evidence and implications for crust–mantle relationships. Earth and Planetary Science Letters 221: 293-308.

Muir RJ, Weaver SD, Bradshaw JD, Eby GN, Evans JA (1995). Geochemistry of the Cretaceous Separation Point batholith, New Zealand: granitoid magmas formed by melting of mafic lithosphere. Journal of the Geological Society of London 152: 689–701.

Najafi A, Karimpour MH, Ghaderi M, Stern CR, Farmer L (2014). U-Pb zircon geochronology, Rb-Sr and Sm-Nd isotope geochemistry, and petrogenesis of granitiod rocks at Kaje prospecting area, northwest Ferdows: Evidence for upper Cretaceous magmatism in Lut block. Journal of Economic Geology 6: 107-135 (in Persian with English abstract).

NIOC (National Iranian Oil Company) (1977). Geological Map of Iran, Scale 1:1000000. Sheets No. 3 (northeast) and 6 (southeast).

Omrani H, Moazzen M, Oberhänsli R, Altenberger U, Lange M (2013). The Sabzevar blueschists of the north-central Iranian microcontinent as remnants of the Neotethys-related oceanic crust subduction. International Journal of Earth Sciences 102: 1491–1512.

Omrani H, Moazzen M, Oberhansli R (2018). Geodynamic evolution of the Sabzevar Zone, north of the Central Iranian Microcontinent. Mineralogy and Petrology 112: 65-83.

Pang KP, Chung SL, Zarrinkoub MH, Khatib MM, Mohammadi SS et al. (2013). Eocene-Oligocene post collisional magmatism in the Lut–Sistan region, eastern Iran: Magma genesis and tectonic implications. Lithos 180-181: 234-251.

Pearce JA, Harris NBW, Tindle AG (1984). Trace element discrimination diagrams for the tectonic interpretation of granitic rocks. Journal of Petrology 25: 956–983.

Peccerillo A, Lustrino M (2005). Compositional variations of Plio-Quaternary magmatism in the circum-Tyrrhenian area: Deep versus shallow mantle processes. Special Paper 388: Plates, Plumes and Paradigms. Geological Society of America 421–434.

Peccerillo A, Taylor SR (1976). Geochemistry of Eocene calc–alkaline volcanic rocks from the Kastamonou area, Northern Turkey. Contributions to Mineralogy and Petrology 58: 63–81.

Petford N, Atherton M (1996). Na-rich partial melts from newly underplated basaltic crust: the Cordillera Blanca Batholith, Peruvian Journal of Petrology 37: 1491–1521.

Prouteau G, Scaillet B, Pichavant M, Maury R (2001). Evidence for mantle metasomatism by hydrous silicic melts derived from subducted oceanic crust. Nature 410: 197–200.

Rahmani F, Mackizadeh MA, Noghreyan M, Marchesi C, Garrido CJ (2020). Petrology and geochemistry of mafic and ultramafic cumulate rocks from the eastern part of the Sabzevar ophiolite (NE Iran): Implications for their petrogenesis and tectonic setting. Geoscience Frontiers 11: 347–2364.

Rapp RP, Watson EB (1995). Dehydration melting of metabasalt at 8–32 kbar: implications for continental growth and crust-mantle recycling. Journal of Petrology 36: 891–931.

Rezaei-Kahkhaei M, Kananian A, Esmaeily D, Asiabanha A (2010). Geochemistry of the Zargoli granite: Implications for development of the Sistan Suture Zone, southeastern Iran. Island Arc 19: 259–276.

Richards JP, Spell T, Rameh E, Razique A, Fletcher T (2012). High Sr/Y magmas reflect arc maturity, high magmatic water content, and porphyry Cu ± Mo ± Au potential: examples from the Tethyan arcs of Central and Eastern Iran and Western Pakistan. Economic Geology 107: 295–332.

Rollinson HR 1(993). Using Geochemical Data: Evaluation, Presentation, and Interpretation. Longman Science and Technical, 352p.

Rossetti F, Nasrabady M, Vignaroli G, Theye T, Gerdes A et al. (2010). Early Cretaceous migmatitic mafic granulites from the Sabzevar range (NE Iran): implications for the closure of the Mesozoic peri-Tethyan Oceans in central Iran. Terra Nova 22: 26–34.

Saccani E, Delavari M, Beccaluva L, Amini SA (2010). Petrological and geochemical constraints on the origin of the Nehbandan ophiolitic complex (eastern Iran): Implication for the evolution of the Sistan Ocean. Lithos 117: 209-228.

Sajona FG, Maury RC, Prouteau G, Cotton J, Schiano P et al. 2000. Slab melt as metasomatic agent in island arc magma mantle sources, Negros and Batan (Philippines). Island Arc 9: 472–486.

Salati E, Karimpour MH, Malekzadeh Shafaroudi A, Haidarian Shahri MR, Farmer L et al. (2013). U-Pb zircon geochronology, Sr-Nd isotope geochemistry, and petrogenesis of oxidant granitoids at Keybarkuh, southwest of Khaf. Journal of Economic Geology 4: 285-301 (in Persian with English abstract).

Samiee S, Karimpour MH, Ghaderi M, Haidarian Shahri MR, Klötzli U et al. (2016). Petrogenesis of subvolcanic rocks from the Khunik prospecting area, south of Birjand, Iran: Geochemical, Sr–Nd isotopic and U–Pb zircon constraints. Journal of Asian Earth Sciences 115: 170–182.

Seghedi I, Downes H (2011). Geochemistry and tectonic development of Cenozoic magmatism in the Carpathian-Pannonian region. Gondwana Research 20: 655-672.

Sengör AMC, Natalin BA (1996). Paleotectonics of Asia: fragment of a synthesis. In: An Y, Harrison TM (eds) The Tectonic Evolution of Asia. Cambridge University. Press, Cambridge 486–640.

Shabanian E, Acocella V, Gioncada A, Ghasemi H, Bellier O (2012). Structural control on volcanism in intraplate post collisional settings: Late Cenozoic to Quaternary examples of Iran and Eastern Turkey. Tectonics 31: 1-25.

Shafaii Moghadam H, Corfu F, Chiaradia M, Stern RJ, Ghorbani G (2015). Sabzevar Ophiolite, NE Iran: Progress from embryonic oceanic lithosphere into magmatic arc constrained by new isotopic and geochemical data. Lithos 210-211: 224-241.

Shafaii Moghadam H, Rossetti F, Lucci F, Chiaradia M, Gerdes A et al. (2016). The calc-alkaline and adakitic volcanism of the Sabzevar structural zone (NE Iran): Implications for the Eocene magmatic flare–up in Central Iran. Lithos. 248–251: 517–535.

Shafaii Moghadam H, Stern R (2015). Ophiolites of Iran: Keys to understanding the tectonic evolution of SW Asia: (II) Mesozoic ophiolites. Journal of Asian Earth Sciences 100: 31–59.

Shojaat B, Hassanipak AA, Mobasher K, Ghazi AM (2003). Petrology, geochemistry and tectonics of the Sabzevar ophiolite, North Central Iran. Journal of Asian Earth Sciences 21: 1053–1067.

Soffel HC, Davoudzadeh Rolf MC, Schmidt S (1996). New palaeomagnetic data from Central Iran and a Triassic palaeoreconstruction. Geologische Rundschau 85: 293–302.

Stampfli GM, Borel GD (2002). A plate tectonic model for the Paleozoic and Mesozoic constrained by dynamic plate boundaries and restored synthetic oceanic isochrones. Earth and Planetary Science Letters. 196: 17-33.

Stampfli GM, Borel GD (2004). The transmed transects in space and time: constraints on the paleotectonic evolution of the Mediterranean Domain, in Cavazza, W., Roure, F., Spakman, W., Stampfli, G.M., Ziegler, P., eds., the transmed atlas: the Mediterranean region from Crust to Mantle. Springer-verlag, p. 53–80.

Stern RJ, Shafaii Moghadam H, Pirouz M, Mooney W (2021). The geodynamic evolution of Iran. Annual Review of Earth and Planetary Sciences 49: 9-36.

Stern CR, Kilian R (1996). Role of the subducted slab, mantle wedge and continental crust in the generation of adakites from the Andean Austral volcanic zone. Contributions to Mineralogy and Petrology 123: 263– 281.

Stöcklin J (1976). Main structural zones recognized in the Alpine Ranges of Iran, Afghanistan, Pakistan and Pamir-Karakorum West Himalayan region: United Nations Development Program.

Sun S-S, Mcdonough WF (1989). Chemical and isotopic systematics of oceanic basalts: implications for mantle composition and processes. In: Saunders, A.D., Norry, M.J. (eds) Magmatism in the Ocean Basins. Journal of the Geological Society of London. 42: 313–345.

Tirrul R, Bell IR, Griffis RJ, Camp VE (1983). The Sistan suture zone of eastern Iran. Geological Society of America Bulletin 94: 134–150.

Verdel C, Wernicke BP, Hassanzadeh J, Guest B (2011). A Paleogene extensional arc flare-up in Iran. Tectonics 30: 1–20.

Walker JA, Patino LC, Carr MJ, Feigenson MD (2001). Slab control over HFSE depletions in central Nicaragua. Earth and Planetary Science Letters 192: 533–543.

White WM, Patchett J (1984). Hf–Nd–Sr isotopes and incompatible element abundances in island arcs: implications for magma origins and crust–mantle evolution. Earth and Planetary Science Letters 67: 167–85.

Xiao L, Clemens JD (2007). Origin of potassic (C-type) adakite magmas: experimental and field constraints. Lithos 95: 399–414.

Younesi S, Hosseinzadeh MR, Moayyed M Maghsoudi A (2016). Investigation of geology, petrology and petrogenesis of igneous rocks from the Mahour Mining exploration area, west Dehsalm: Implication for Lut tectonomagmatic setting. Geosciences Scientific Quarterly Journal 25: 176-198 (in Persian with English abstract).

Zarrinkoub MH, Chung S-L, Chiu H-Y, Mohammadi S, Khatib M et al. (2010). Zircon U–Pb age and geochemical constraints from the northern Sistan suture zone on the Neotethyan magmatic and tectonic evolution in eastern Iran. Abstract to GSA Conference on "Tectonic Crossroads: Evolving Orogens in Eurasia–Africa–Arabia", Oct. 4–8, 2010, Ankara, Turkey.

Zarrinkoub MH, Chung SL, Mohammadi SS, Khatib MM (2011). Geochemistry, petrology and zircon U–Pb dating for Bibi Maryam granitoid, NE of Nehbandan, east of Iran. Journal of Economic Geology 3: 15–27 (in Persian with English abstract).

Zarrinkoub, M.H., Pang, K.N., Chung, S.L., Khatib, M.M., Mohammadi, S.S., Chiu, H.Y., Lee, H.Y., 2012. Zircon U–Pb age and geochemical constraints on the origin of the Birjand ophiolite, Sistan suture zone, eastern Iran. Lithos 154, 392-405.

Zindler, A., Hart, S.R., 1986. Chemical geodynamics. Ann. Rev. Earth Plant. Sci. 14, 493–571.